Calculating Absorption and Fluorescence Spectra for Chromophores in Solution with Ensemble Franck-Condon Methods

Ajay Khanna, Sapana V. Shedge, Tim J. Zuehlsdorff, and Christine M. Isborn^{1, a)}

Chemistry and Biochemistry, University of California Merced, Merced, California 95343,
United States

Department of Chemistry, Organ State University, Compilie, Organ 97321

²⁾ Department of Chemistry, Oregon State University, Corvallis, Oregon 97331, United States

(Dated: 29 August 2024)

Accurately modeling absorption and fluorescence spectra for molecules in solution poses a challenge due to the need to incorporate both vibronic and environmental effects, as well as the necessity of accurate excited state electronic structure calculations. Nuclear ensemble approaches capture explicit environmental effects, Franck-Condon methods capture vibronic effects, and recently introduced ensemble-Franck-Condon approaches combine the advantages of both methods. In this study, we present and analyze simulated absorption and fluorescence spectra generated with combined ensemble-Franck-Condon approaches for three chromophore-solvent systems and compare them to standard ensemble and Franck-Condon spectra, as well as to experiment. Employing configurations obtained from ground and excited state ab initio molecular dynamics, three combined ensemble-Franck-Condon approaches are directly compared to each other to assess the accuracy and relative computational time. We find that the approach employing an average finite-temperature Franck-Condon lineshape generates spectra nearly identical to the direct summation of an ensemble of Franck-Condon spectra at one-fourth of the computational cost. We analyze how the spectral simulation method, as well as the level of electronic structure theory, affects spectral lineshapes and associated Stokes shifts for 7-nitrobenz-2-oxa-1,3-diazol-4-yl (NBD) and Nile Red in dimethyl sulfoxide (DMSO), and 7-methoxy coumarin-4-acetic acid (7MC) in methanol. For the first time, our studies showcase the capability of combined ensemble-Franck-Condon methods for both absorption and fluorescence spectroscopy and provide a powerful tool for simulating linear optical spectra.

I. INTRODUCTION

Optical spectroscopy plays a pivotal role in understanding the properties of molecules, where absorption and fluorescence spectra act as reporters for local environments and vibronic coupling through their energies, spectral widths, shapes, and Stokes shifts. Simulations of optical spectroscopy serve as a crucial bridge between experimental results and electronic-level understanding of molecular behavior. Developing models that can effectively capture both explicit environmental effects and vibronic contributions remains a critical challenge in linking experimental spectra with molecular properties.

Traditional computational methods for linear spectroscopy simulation have predominantly focused on incorporating vibronic effects through Franck-Condon (FC) spectral simulations^{1–17} using either an adiabatic Hessian^{7,18,19} or a vertical gradient approach¹² for efficiency. In practice, harmonic potential energy surfaces are generally assumed within the FC approach as the harmonic oscillator nuclear wave functions are readily available upon geometry optimization and normal mode analysis. The FC methods often model solvent effects implicitly, utilizing polarizable continuum models^{20–26} to approximate the influence of the surrounding medium. This harmonic FC approach works

well for rigid molecules or systems with weak solvent interactions. However, the absence of direct solute-solvent interactions and the harmonic treatment of the potential energy surfaces can lead to more narrow spectra than observed experimentally. 27,28

Explicit solvent effects are traditionally incorporated into spectral simulations by employing a nuclear ensemble approach.^{29–38} This method involves sampling chromophore-solvent configurations, generally through a molecular dynamics (MD) trajectory, and naturally captures vibrational degrees of freedom of the chromophore. This approach does not incorporate vibronic effects, ¹⁹ often leading to poor spectral shape. The ensemble approach has seen limited application in simulating fluorescence spectra, ^{32,39–43} likely due to the computational demands of performing excited state molecular dynamics to obtain chromophore-solvent configurations on the excited state potential energy surface. There are multiple advantages of the nuclear ensemble approach, such as being able to sample anharmonic regions of the potential, the ease of including effects from higher-lying excited states, capturing inhomogeneous broadening due to explicit interactions with solvent, and accounting for temperature effects of both the chromophore and solvent via finite temperature MD. 33,44,45

Some recent approaches to simulating absorption spectra have made progress in capturing both specific environmental and vibronic effects through the use of MD sampling of chromophore-environment configurations. For example, employing a cumulant expansion

a) cisborn@ucmerced.edu

for the ensemble average of the time-ordered exponential of the linear response function⁴⁶ treats chromophore vibrational and environmental degrees of freedom on equal footing, allowing vibronic absorption spectra to be generated from energy gap correlation function computed along an MD trajectory. 47-58 Molecular dynamics, along with snapshot clustering for unique features, has also been exploited within a variational and perturbative approach to spectroscopy.⁵⁹⁻⁶¹ An alternative approach based on the separation of classical (soft) and quantum (stiff) nuclear degrees of freedom expresses the absorption spectrum as a conformational integral of vibronic spectra of the stiff coordinates. 62,63 The approach developed by some of the authors of the present work is similar in spirit, where vibronic spectra of the chromophore are generated within a frozen environment in order to combine features of both the ensemble and Franck-Condon approaches, creating hybrid ensemble-Franck-Condon (E-FC) approaches that capture both explicit environment and vibronic effects. 28,64-67 In previous work,⁶⁷ we have outlined variations of the E-FC approach with differing levels of approximation and corresponding computational cost, and shown good agreement with experiment for the simulated absorption spectral shapes of chromophores in various explicit solvent environments.

In this study, we compare three E-FC methods introduced previously and, for the first time, extend these approaches to the simulation of fluorescence spectra. This is the first study in which these methods have been directly compared to each other and the first in which they have been used to model fluorescence. We employ both ground and excited state ab initio molecular dynamics (AIMD) to sample chromophore-solvent configurations and compare the resulting ensemble, implicit solvent Franck-Condon, and E-FC absorption and fluorescence lineshapes. To showcase the performance of these spectroscopy methods, they are applied to three well-known fluorophores: 7-nitrobenz-2-oxa-1,3-diazol-4-yl (NBD), Nile Red (NR), and 7-methoxy coumarin-4-acetic acid (7MC).

II. THEORY

Here we present the theory of computational methods used in this study for modeling the linear optical spectra of molecules in solution, including the nuclear ensemble approach, $^{29-32}$ the Franck-Condon approach, $^{1-17}$ and the combined ensemble-Franck-Condon approaches. $^{28,64-67}$ For simplicity, we only account for two electronic states in spectral calculations: the initial reference electronic state, i, and the final electronic state, f, where the reference state is the ground state for absorption spectra, and the reference state is the excited state for emission spectra. We assume Born-Oppenheimer dynamics for both S_0 and S_1 , and therefore do not consider any contributions from nonadiabatic effects 68,69 . Note that our ex-

pressions for absorption cross-sections are scaled by the frequency ω , and emission cross-sections are scaled by $\omega^3,^{70,71}$ with other references suggesting that the scaling should be $\omega^4.^{72-74}$ In this work, we present a comparison of spectral lineshapes with the transformation from spectral intensity to lineshape intensity given in the computational details.

A. The Nuclear Ensemble Approach

In the nuclear ensemble approach, the electronic spectra are simulated using molecular configurations, here called snapshots, that we sample from different points in time during an MD trajectory at a specified temperature. For absorption, ground state MD is performed, followed by calculations of vertical excitation energy (VEE) and oscillator strength for each snapshot. For emission, excited state MD is performed, with the energy gap calculations on these snapshots representing the vertical deexcitation energy (VDE). To obtain the final optical spectrum, often a Gaussian function dresses the bare vertical energies. The linear absorption and emission cross-sections using the ensemble approach are then obtained as,

$$\sigma^{\text{ens}}(\omega;T) \propto \frac{1}{N_{\text{snaps}}} \sum_{j=1}^{N_{\text{snaps}}} \omega_{if}^{\beta}(\boldsymbol{R_{j}^{i}};T) |\mu_{if}(\boldsymbol{R_{j}^{i}};T)|^{2} \times \mathcal{N}(\omega - \omega_{if}(\boldsymbol{R_{j}^{i}};T),s),$$

$$(1)$$

where $f_{if} \propto \omega_{if}(\boldsymbol{R_j^i};T)|\mu_{if}(\boldsymbol{R_j^i};T)|^2$ is the oscillator strength, ω_{if} is the vertical excitation/de-excitation energy, $\beta=1$ for absorption and $\beta=3$ for emission, and μ_{if} is the transition electric dipole moment between two electronic states of the dye with reference state nuclear configuration $\boldsymbol{R_j^i}$ obtained from an MD trajectory at temperature T. The frequency of the light is given by ω , and N_{snaps} is the number of uncorrelated snapshots from either a ground or excited state MD trajectory. The Gaussian function, \mathcal{N} , is centered at ω_{if} with standard deviation s, a parameter that is often used to account for limited sampling. Some nuclear quantum effects on the optical spectra can be included through the MD sampling by employing a path integral formalism. To However, the spectra generated from the nuclear ensemble approach lack vibronic features and, thus, generally are not the correct shape.

B. The Franck-Condon Approach

The Condon approximation assumes that the nuclear configuration does not change during an electronic transition, leading to the Franck-Condon principle, where the intensity of the electronic transition can be determined from the overlap of the nuclear (vibrational) wave

functions of the initial and final electronic states, creating a vibronic spectrum. The absorption and emission cross-section at a finite temperature (FT) for the FC approach^{8,13} creates an FTFC spectrum given by,

$$\sigma^{FC}(\omega;T) \propto \omega^{\beta} |\mu_{if}^{\text{opt}}(\boldsymbol{R}^{i,\text{opt}})|^{2} \sum_{\nu_{i}} \sum_{\nu_{i}} \rho(\nu_{i},T) |\langle \phi_{\nu_{f}} | \phi_{\nu_{i}} \rangle|^{2} \times \delta \left(\omega_{\nu_{f}} - \omega_{\nu_{i}} \pm \omega\right),$$
(2)

where ω is the frequency of the incident (ω^1) or emitted (ω^3) photon. The Boltzmann distribution of the initial state at temperature T is denoted by $\rho(\nu_i, T)$, and $\phi_{\nu_i}, \phi_{\nu_f}$ are the nuclear vibrational wave functions of the electronic state i and f, and the delta function is placed at the energy of absorption or emission, with + used for absorption and - for emission. The delta function is usually replaced by a Gaussian function, $\mathcal{N}\left(\omega_{\nu_f}-\omega_{\nu_i}\pm\omega,s\right)$, where the standard deviation, s, generally represents the solvent-induced broadening, which is usually chosen in an ad-hoc way but can also be estimated by Marcus theory. 27,79,80 Solvent effects on the optimized geometry and frequencies are frequently included using implicit solvent models such as the polarizable continuum model (PCM). $^{20-25}$

Savings in time for computation of the FTFC spectrum can be achieved using the vertical gradient approach that employs only the normal modes of the ground state optimized structure, ^{81–85} instead of the full adiabatic Hessian that requires the normal mode computation for both the ground and the excited state optimized structures. FC spectral simulations can also account for Herzberg-Teller effects ^{13,86–89}; based on initial tests with both implicit and explicit solvents, we found these effects to be negligible for all three chromophores.

C. Combined Ensemble Franck-Condon (E-FC) Approaches

The nuclear ensemble approach generates spectra that include direct solute-solvent interactions but lack vibronic features, whereas the standard FC approach generates spectra that include vibronic features but lack the effects of direct solute-solvent interactions. A family of computational approaches that combine the advantages of the ensemble approach and the FC approach, which we here call E-FC methods, were introduced in previous work, ^{28,64–67} where we have described these approaches for combining ensemble sampling of the environment with Franck-Condon lineshapes, outlining methods with varying degrees of computational cost. Like the ensemble approach, snapshots of chromophore-environment configurations are first obtained at the desired temperature. Each configuration corresponds to a different local environment; the effects of the environment on the FC lineshape can be captured by freezing the solvent environment and then optimizing the ground and excited

state geometry and computing the normal modes of the chromophore. The three E-FC approaches we've developed to incorporate these local environment effects with vibronic transitions are given in order of decreasing computational cost:

- Summation of the finite temperature FC (FTFC) spectrum obtained for each snapshot in the ensemble (E-sumFTFC). For the adiabatic Hessian FC approach,¹² this method involves the computationally expensive evaluation of ground and excited state normal modes for each snapshot.
- 2. Summation of an FTFC lineshape that is used to dress the vertical excitation/de-excitation energies obtained at optimized geometries of the chromophore in the frozen solvent, where we employ an average FTFC lineshape ($E_{\rm opt}$ -avgFTFC), thus avoiding the costly excited state normal mode calculation for many snapshots.
- 3. Summation of a zero-temperature FC (ZTFC) lineshape that is used to dress the vertical excitation/de-excitation energies obtained at snapshot geometries, where we employ an average ZTFC lineshape (E-avgZTFC), altogether avoiding both the ground state and excited state optimization for many snapshots.

The following sections present the theoretical details for each of these three approaches as we herein, for the first time, directly compare the lineshapes of the approaches and extend the family of methods to model fluorescence spectra. We thus present some slight modifications of our previous expressions so that the energies of absorption and fluorescence spectra are computed on equal footing, allowing the computation of Stokes shifts.

1. Summation of an Ensemble of Finite Temperature Franck-Condon Spectra (E-sumFTFC)

For the E-sumFTFC approach, an FTFC spectrum is computed for each snapshot, and then all FTFC spectra are summed to generate the final absorption or emission spectrum. The inhomogeneous broadening then arises from the different energies of the spectra obtained from the different local environments. The E-sumFTFC absorption and emission spectra are generated as

$$\sigma_{\text{E-sumFTFC}}(\omega, T) = \frac{1}{N_{\text{snaps}}} \sum_{j}^{N_{\text{snaps}}} \sigma_{j}^{\text{FC}}(\omega, T; \boldsymbol{R}_{j}^{i, \text{opt}}; \boldsymbol{R}_{j}^{i, \text{solv}}),$$
(3)

where σ_j^{FC} is the FTFC absorption/emission spectrum of each snapshot computed with optimized chromophore geometry, $R_j^{i,opt}$, in a frozen solvent configuration, $R_j^{i,solv}$

for reference electronic state *i*. Temperature effects of the chromophore are modeled through the population of the vibrational energy levels within the FTFC lineshape function, whereas temperature effects of the solvent are modeled classically using MD. Although straightforward, this E-sumFTFC approach is computationally expensive as within an adiabatic Hessian approach it requires geometry optimization for both ground and excited states, along with computation of the corresponding normal modes.

2. Optimized Ensemble Average Finite Temperature Franck Condon (E_{out}-avgFTFC)pproach

The cost of the E-sumFTFC approach can be reduced by using an average FC lineshape function generated using a small number of snapshots and aligning the lineshape with the VEE/VDEs obtained from the optimized geometries of the chromophore in the frozen solvent. The use of an average FC lineshape is valid if the perturbation introduced by the different local frozen solvent environments present in each snapshot does not significantly alter the shape or displacement of the ground and excited-state potential energy surfaces of the chromophore. The average FTFC lineshape, $\sigma^{\rm avgFTFC}$, is derived by aligning the absorption or emission 0-0 energies, ω_{00} , of individual FTFC spectra. We then scale the area of the lineshape for each snapshot according to the square of the transition dipole computed for the optimized geometry.

Within the E_{opt}-avgFTFC approach, the vibrational frequencies and a full vibronic spectrum are not calculated for each snapshot, and therefore ω_{00} that measures the energy difference between the zero-point energies of the ground and excited state for each snapshot is not available. The question then arises - How will the placement of the average FC lineshape be determined, given that we only have the VEE/VDEs for each snapshot? Generally, the VEE is higher in energy than ω_{00} , and the VDE energy is lower in energy than ω_{00} . For placement of the average FC lineshape for each snapshot at an energy approximating ω_{00} for that snapshot, we determined an energetic shift value as the average value of the difference between the VEE/VDE and ω_{00} for the snapshots used in the average FTFC lineshape calculation: $(\omega_{if} - \omega_{00})_{FC}$. This value is positive for absorption and negative for emission. The average FTFC lineshape is then aligned with its ω_{00} at the value of the vertical excitation/deexcitation energy for each snapshot shifted by $(\omega_{if} - \omega_{00})_{FC}$, and the spectra are summed to create the E_{opt}-avgFTFC spectrum as

$$\sigma_{E_{\text{opt}}-\text{avgFTFC}}(\omega, T) = \frac{1}{N_{\text{snaps}}} \sum_{j}^{N_{\text{snaps}}} \left| \mu_{if}(\boldsymbol{R}_{j}^{i, \text{opt}}; \boldsymbol{R}_{j}^{i, \text{solv}}) \right|^{2} \times \sigma^{\text{avgFTFC}}(\omega - \Delta\omega_{if}, T),$$
(4)

where here $\Delta \omega_{if} = \omega_{if}(\boldsymbol{R}_{j}^{i,\text{opt}};\boldsymbol{R}_{j}^{i,\text{solv}}) - \overline{(\omega_{if} - \omega_{00})}_{\text{FC}}$, with $\omega_{if}(\boldsymbol{R}_{j}^{i,\text{opt}};\boldsymbol{R}_{j}^{i,\text{solv}})$ the VEE/VDE of snapshot j optimized on reference potential i. By using only a small number of snapshots to generate the average FC lineshape, we only perform the geometry optimization for the reference state for the remaining snapshots, and ground and excited state normal mode calculation for each snapshot can be avoided, thus significantly reducing the computation cost.

3. Ensemble Average Zero Temperature Franck Condon (E-avgZTFC) Approach

A further reduction in the computational cost can be achieved by avoiding geometry optimization of the ensemble of snapshots altogether and instead dressing the shifted VEE/VDEs of the ensemble of solute-solvent configurations directly with an average zero-temperature (ZT) FC lineshape. This E-avgZTFC approach accounts for temperature classically in the vibrational degrees of freedom of both the chromophore and the solvent, as there is no population of the vibrational energy levels in the zero-temperature FC lineshape. The average ZTFC lineshape is generated through the same procedure as the average FTFC lineshape, with the alignment of the 0-0 transitions. The linear optical spectrum using this approach is then obtained as,

$$\sigma_{\text{E-avgZTFC}}(\omega, T) = \omega^{\beta} \frac{1}{N_{\text{snaps}}} \sum_{j}^{N_{\text{snaps}}} \left| \mu_{if}(\boldsymbol{R}_{j}^{i}; T) \right|^{2} \times \sigma^{\text{avgZTFC}}(\omega - \Delta\omega_{if}, T),$$
(5)

where here $\Delta \omega_{if} = \omega_{if}(\boldsymbol{R}_{j}^{i}) - \overline{(\omega_{if} - \omega_{00})}_{FC}$, with $\omega_{if}(\boldsymbol{R}_{j}^{i})$ the VEE/VDE of unoptimized snapshot j obtained from the MD trajectory on the reference PES i. Although this E-avgZTFC approach is the most computationally affordable of all three E-FC methods, this approach double-counts the zero-point vibrational motion of the chromophore: once from the sampling of vibrational degrees of freedom in the nuclear ensemble and then again in the zero-temperature nuclear wave packet of the ZTFC lineshape. This double-counting may result in overly broad spectra.

III. COMPUTATIONAL DETAILS

Our computational strategy for generating implicit solvent FTFC, ensemble, and E-FC spectra is shown pictorially in Figure 1. To generate and then align spectra in the combined ensemble-Franck-Condon approach, we follow four steps:

(A) Sampling configurations using AIMD where we treat the chromophore quantum mechanically (with QM) and the solvent with fixed molecular mechanical (MM) point charges

- (B) Performing QM/MM electronic structure calculations on AIMD snapshots (computing excitation energies, geometry optimization, and normal modes)
- (C) Generating spectra using combined ensemble-Franck-Condon (E-FC) methods
- (D) Aligning spectral lineshapes for better comparison with experiment

A. Sampling Configurations Using Ab Initio Molecular Dynamics

The starting system is a droplet with an initial solvent radius of 37 Å around the chromophore. For initial thermalization and equilibration before the AIMD trajectory, the generalized amber force field version 2 (GAFF2)⁹³ was parameterized for the ground and excited state potential energy surfaces using the RESP procedure for dyes; see Supplementary Material, section S1, for additional details. Restrained classical force field MD⁹⁴ was performed without periodic boundary conditions, followed by the use of the TeraChem-AMBER interface⁹⁵ for AIMD QM/MM simulations, wherein only the chromophore is treated with QM, while the solvent is treated with parameterized GAFF2, with the MM point charges coupled to the QM region with an electrostatic embedding approach. 96-98. During the AIMD simulations, the temperature of the system was maintained at 300 K using the Berendsen⁹⁹ thermostat with a time constant of 1 ps for the heat bath coupling. For ground state AIMD, the CAM-B3LYP range-separated density functional and the 6-31G(d) basis set was used for the chromophore and for the excited state AIMD, we use the Tamm-Dancoff approximation $(TDA)^{101}$ to $TDDFT^{102}$ with the same level of theory. For both the ground and excited state trajectories, the initial 10 ps of the AIMD QM/MM trajectories were discarded to let the system equilibrate with the new Hamiltonian. After the system was equilibrated, a few snapshots were chosen randomly to act as the starting points for separate independent AIMD simulations. These simulations are used for the production run. From the independent trajectories, a total of 100 uncorrelated snapshots were obtained, separated by at least 200 fs.

B. Performing Electronic Structure Calculations

Once an ensemble of uncorrelated snapshots was obtained, for each snapshot, we performed calculations of the VEE or VDE, ground or excited state geometry optimization, and corresponding frequencies. Each snapshot is divided into three layers: a central dye that is optimized during the ground or excited state geometry optimizations and is treated with QM, a 5 Å region of frozen solvent from the geometric center of the dye treated with

QM but excluded from optimization, and a 27 Å region of MM fixed point charge solvent providing an electrostatic environment to the QM region. Thus, the QM region for all snapshot calculations is the chromophore plus 5 Å of solvent to fully account for chromophore-solvent polarization and charge transfer.

For all electronic structure calculations, we use the CAM-B3LYP/6-31G(d) level of theory with empirical dispersion accounted via the D3 version of Grimmes dispersion. 103 Because the TDA usually provides excitation energy and vibronic lineshapes similar to TDDFT and is computationally cheaper than TDDFT¹⁰⁴, we use the TDA within TDDFT for the excited state properties. Comparisons between TD and TDA are also provided in the Supplementary Material for each dye. The performance of the various density functionals for excited state properties, including fluorescence, has been evaluated previously, with range-separated hybrid functionals found to be superior. 105 Here we focus on the absorption and fluorescence vibronic lineshapes and provide comparisons for FC spectra using CAM-B3LYP¹⁰⁰, LC- ω HPBE¹⁰⁶⁻¹⁰⁸, and M06-2x¹⁰⁹ density functionals in both implicit and explicit solvents. These results are detailed in the SM for each dye.

For geometry optimization in explicit QM solvent and VEE/VDE calculations, the 2020 development version of TeraChem 110 was used. Frequency calculations in frozen QM solvent and vibronic spectra calculations were carried out using a developmental version of Gaussian16. 111 The integral equation formalism for PCM $^{112-116}$ as implemented in Gaussian16 was used for modeling solvent effects on implicit solvent FC absorption and emission spectra.

C. Generating Spectra Using Combined Ensemble-Franck-Condon (E-FC) Methods

For all vibronic FC spectra, for both implicit and explicit solvent environments, the time-dependent implementation of one photon absorption and emission procedure^{4–17} was employed with the default adiabatic Hessian model as implemented in the development version of the Gaussian16 electronic structure program. A temperature of 300 K was used for the finite temperature FC spectra. Two advantages of the time-dependent FC implementation are that zero temperature spectra are obtained along with finite temperature spectra at no additional computational cost, and no approximations are made when summing over contributions for combination modes.⁸⁶

The average FC lineshapes were generated using ten randomly selected snapshots and aligning their 0-0 transitions for avg₁₀FTFC and avg₁₀ZTFC methods. We tested the robustness of the lineshape generated with the randomly selected snapshots, see Figure S1, finding ten snapshots to be adequate.

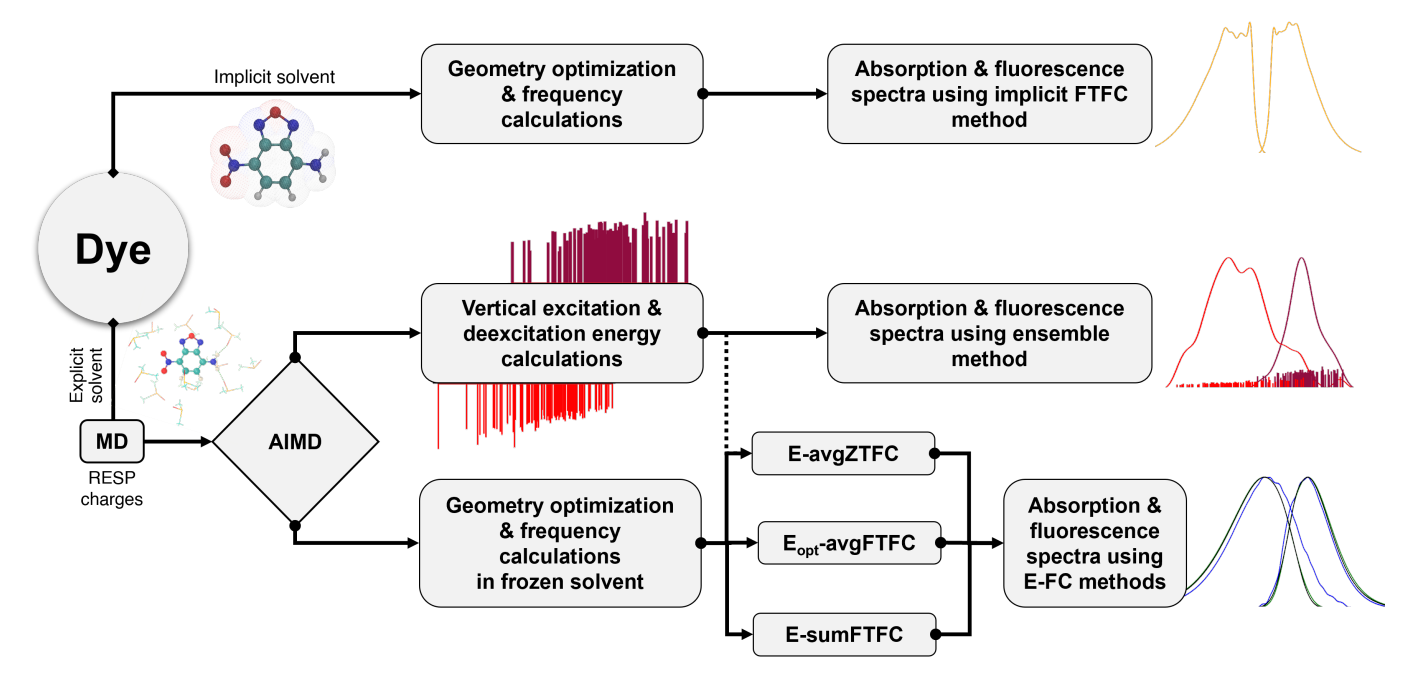


FIG. 1. Computational procedure for modeling absorption and fluorescence spectra of dyes in an implicit and explicit solvent environment using various spectroscopy methods.

D. Spectral Simulation Parameters and Alignment

For equivalent comparison of spectra, we transform the experimental and simulated spectra to energy-independent lineshapes as described in the Supplementary Material, section S2. This transformation will affect the value of the Stokes shift; herein, we report the Stokes shift from the lineshapes after the transformation. The Stokes shift measures the difference between the energy of excitation and deexcitation at corresponding band maxima. We follow this approach for reporting the Stokes shift using the maxima of the computed spectra. However, this definition can become inconsistent when dealing with multiple maxima or jagged spectra, complicating the comparison of Stokes shift values.

We also report the full-width-half-maxima (FWHM) of our computed lineshapes to compare with the experiment. This value is dependent on our choice of broadening factor. A Gaussian lineshape function with a broadening factor of 600 cm⁻¹ was used to generate the ensemble lineshapes. For both implicit and explicit solvent FTFC spectra, the Gaussian 16 default half width half maximum (HWHM) value of 135 cm⁻¹ was used as the FC broadening factor. Although the hybrid E-FC spectroscopy methods include inhomogeneous broadening in the lineshapes, due to the use of a limited number of snapshots to calculate the spectra, the final E-FC lineshapes, especially in zero-temperature spectra, can be noisy. Using 135 cm⁻¹ HWHM results in smoother lineshapes while maintaining the overall lineshape width, ^{62,77} see further details in SM, Section S5.

This study aims to compare the computed lineshape

generated for a single bright state transition using different spectroscopy methods. Therefore, we have normalized the lineshapes based on their maximum intensities. We also display all computed lineshapes energetically shifted to align with the experimental lineshapes. For the ensemble absorption and emission lineshapes, the average values of the vertical excitation and deexcitation energies are aligned with the experimental lineshape maxima. For vibronic spectra, we aligned the lineshape maxima, except for more jagged spectra, where averaged band maxima were used to determine alignment. This averaging procedure selects the peaks within 80% of the first maximum and then computes the average energy of these peaks. For all computed lineshapes, the applied energy shift is given in the main manuscript, and the unshifted lineshapes are shown in the Supplementary Material, Figure S3.

IV. RESULTS AND DISCUSSION

Our study involves three well-known fluorophores: 7-nitrobenz-2-oxa-1,3-diazol-4-yl (NBD) and Nile Red (NR) in dimethyl sulfoxide (DMSO), and 7-methoxy coumarin-4-acetic acid (7MC) in methanol; see Figure 2 for chromophore structures. These fluorophores are commonly employed as fluorescent probes for labeling biological substrates. ¹¹⁷⁻¹²² The experimental absorption and emission data for NBD and NR were obtained from Tosi et al., ¹²³ whereas spectra for 7MC in methanol were taken from the PhotochemCAD database. ^{124,125} The experimental spectra and corresponding transformed line-

shapes are shown in Figure S3. Below, we present simulated spectra for each chromophore, and then we analyze relative computational timings for the E-FC methods. For each chromophore, we consider only the low-lying bright state in our simulated spectra. If two electronic states are nearly degenerate, a dark state can mix with the bright state of interest, and then an approach that accounts for nonadiabatic coupling between excited states is necessary for simulating the spectra. ^{126,127} A discussion of such state mixing is presented for each chromophore in the SM.

FIG. 2. Chemical structures of the three chromophores studied in this work: 7-nitrobenz-2-oxa-1,3-diazol-4-yl (NBD), Nile red (NR), and 7-methoxy coumarin-4-acetic acid (7MC).

A. NBD in DMSO

NBD and its derivatives, due to high sensitivity to the polarity of the environment, are routinely used as fluorescent dyes. $^{128-132}$ In aprotic solvents like DMSO, NBD acts as a hydrogen bond donor via the chromophore's NH $_2$ group, potentially forming two hydrogen bonds with the oxygen atom in the DMSO solvent. For the first excited state, which is also the bright state of interest here, there is a partial intramolecular charge-transfer character driving the observed fluorescence. 117,133,134

The FWHM of experimental¹²³ absorption and emission lineshapes (after the scaling correction discussed in Eqs. 6-7) are 0.341 and 0.400 eV, respectively, suggesting potentially an increase in the flexibility of the molecule in the excited state or an increase in the strength of the chromophore-solvent interactions compared to the ground state. The lineshape Stokes shift is moderate at 0.334 eV.

From the 100 uncorrelated snapshots from the ground and excited state AIMD trajectories, we performed VEE/VDE calculations on these snapshots for use in

TABLE I. NBD in DMSO: FWHM, applied energy shift, and Stokes shift from experiment, ensemble, implicit FTFC, and E-FC methods for absorption and emission lineshapes. All values are given in eV.

Methods	Abs FWHM	Abs Ems WHM FWHM		Ems Energy Shift	Stokes Shift
Exp_{LS}	0.341	0.400	-	-	0.334
Implicit	0.330	0.381	0.663	0.819	0.123
Ensemble	0.155	0.336	0.901	0.575	0.731
Ensemble_{Opt}	0.154	0.218	0.925	0.636	0.668
E-avg ₁₀ ZTFC	0.379	0.557	0.810	0.546	0.635
E_{opt} -avg ₁₀ FTFC	0.380	0.536	0.782	0.573	0.580
E-sum ₁₀₀ FTFC	0.370	0.532	0.798	0.582	0.588

both ensemble and E-ZTFC spectra calculations. After optimizing the excited state geometries in the field of the frozen QM solvent, we observe a significant decrease in the energy fluctuations, see Figure S5, suggesting that these large fluctuations on the excited state are due to motions of the chromophore degrees of freedom rather than increased strength of chromophore-solvent interactions. Next, we analyze these energies in the context of ensemble absorption and emission spectra.

Figure 3 shows the experimental and computed absorption and fluorescence spectral lineshapes for NBD in DMSO. The computed lineshapes are shifted on the energy axis, as discussed in the computational details, for better comparison of lineshapes. Table I gives the FWHM, applied energy shifts, and Stokes shift values for all lineshapes. See the SM for unshifted spectral lineshapes.

The spectra generated using the nuclear ensemble approach, as shown in Figure 3a, reveal that the VDEs exhibit larger fluctuations than the VEEs, resulting in an emission spectrum that is significantly broader than the absorption spectrum. This is evidenced by the standard deviation of the energies and the FWHM of the emission spectrum being almost twice as large as those of the absorption spectrum, see Table I. We also analyzed the impact of chromophore-only configurations on spectral broadening and found that chromophore motion is the main driving factor for VDE distribution. Please refer to SM, Section S6 and Figure S6 for a detailed discussion.

A Stokes shift can be computed from the ensemble of VEE/VDEs, but this value should not be rigorously compared to experimental lineshape maxima as spectra generated from the ensemble approach do not include vibronic contributions, which can affect the position of the maxima. Taking the difference between the ensemble spectral maxima gives a value of 0.731 eV, significantly larger than the experimental lineshape Stokes shift value of 0.334 eV. In contrast, the difference in the VEE at the ground state geometry and the VDE at the excited state geometry, both with implicit solvation for the respective state, is only 0.357 eV, as mentioned previously. We can isolate the origin of this difference by comparing VEE and VDE differences. The average VEE value from the

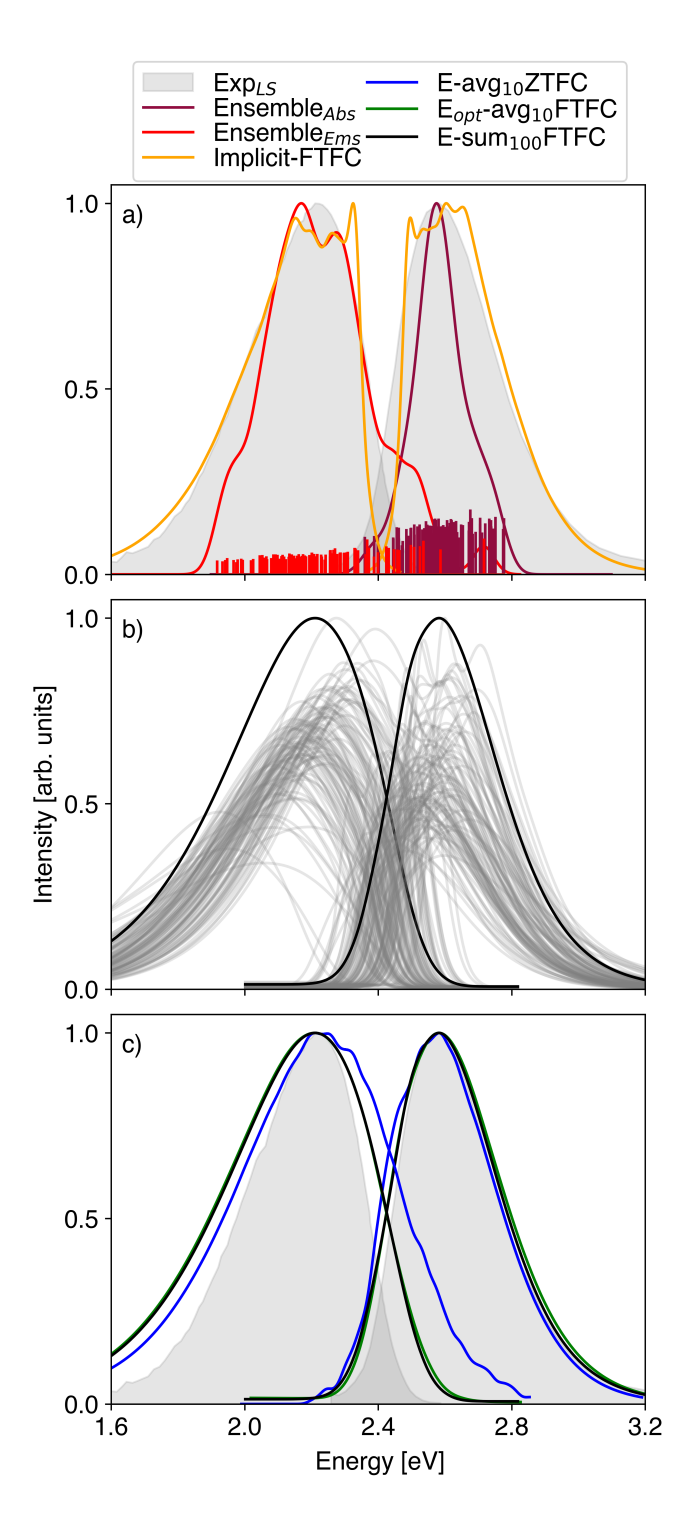


FIG. 3. Absorption and fluorescence lineshapes of NBD in DMSO: Filled gray spectra are experimental lineshapes, transformed from Ref. 123. a) Ensemble and implicit solvent FTFC methods, b) E-sum₁₀₀FTFC and individual FTFC spectra, and c) E-avg₁₀ZTFC, E_{opt}-avg₁₀FTFC, and E-sum₁₀₀FTFC lineshapes. All lineshapes are shifted energetically to align with the experimental lineshape maxima.

explicit solvent snapshots is 3.483 eV, and the implicit solvent-optimized geometry VEE value is 3.605 eV, 0.122

eV higher. In contrast, the average VDE value from the explicit solvent snapshots is 2.786 eV and the implicit solvent-optimized geometry VDE value is 3.248 eV, 0.462 eV higher. There is clearly a much larger discrepancy in VDE compared to VEE, suggesting a substantial change in electronic structure for the explicitly solvated excited state AIMD snapshots compared to the implicitly solvated excited state optimized geometry. This shift to lower VDE for the explicitly solvated excited state is responsible for the overly large computed Stokes shift with the ensemble method.

The implicit solvent FTFC spectral lineshapes, shown in Figure 3a, display asymmetry from the vibronic tail and show relatively good agreement with the experimental lineshape (FWHM values of 0.330 and 0.381 eV for absorption and emission, respectively), with both absorption and fluorescence being slightly underestimated in width by 0.011 eV and 0.019 eV, respectively. The computed Stokes shift determined from the lineshape spectral maxima is 0.123 eV, thus significantly underestimated compared to the experimental value of 0.334 eV (see Table I). Overall, the implicit solvent model predicts toonarrow spectral lineshapes and underestimates the Stokes shift when we employ the default broadening factor of 135 $\rm cm^{-1}$.

We now turn to the main focus of this work and the spectra generated with the combined ensemble-Franck-Condon methods. The results obtained from the ensemble and implicit solvent FTFC approaches highlight the significance of explicit environmental interactions and vibronic contributions. The E-FC methods incorporate both of these effects.

Examining lineshapes computed with the E-sumFTFC approach, Figure 3b, we note that both absorption and fluorescence spectra are generated using the same one hundred snapshots obtained from the ground and excited state AIMD as in the ensemble spectral simulations but with the ground and excited state geometry optimizations and frequency calculations performed with frozen QM solvent. The individual FTFC spectra (thin gray lines) show a significant degree of variability in the lineshape and position, confirming the importance of explicit environmental interactions on the resulting vibronic spectrum. The FWHM of individual explicit solvent FTFC spectra, see Figure 4, range between 0.260 and 0.780 eV. with an average FWHM value of 0.366 eV for absorption and 0.514 eV for emission. These average values are larger than the FWHM values for the implicit solvent FTFC spectra of 0.354 and 0.458 eV, suggesting that for NBD, the QM explicit solvent environment leads to stronger vibronic coupling than the implicit solvent environment, even more so for fluorescence.

The summed FTFC spectra create the E-sum $_{100}$ FTFC absorption and emission spectra, black lines in Figure 3b and c, which are broader than their implicit solvent FTFC counterparts, with smoothed-out vibronic features. Overall, the E-sum $_{100}$ FTFC absorption lineshape gives good agreement with the experimental absorption

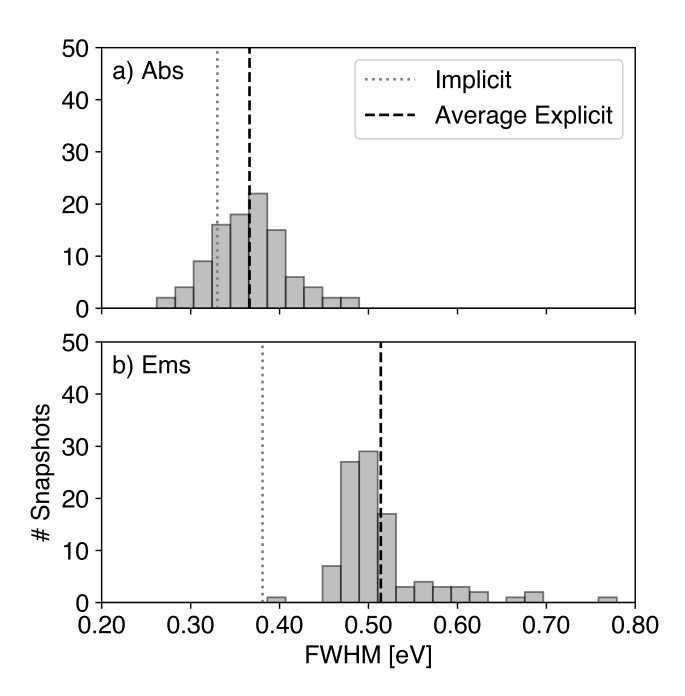


FIG. 4. Frequency distribution of a) absorption and b) emission vibronic lineshape FWHM values of NBD in DMSO. The dotted gray lines correspond to the FWHM of the implicit solvent FTFC spectra (Abs: 0.330 eV, Ems: 0.381 eV). The dashed black lines represent the average values of the FWHM of the explicit solvent FTFC spectra (Abs: 0.366 eV, Ems: 0.514 eV).

lineshape, see Figure 3c, with a slight overestimation of the FWHM value. In contrast, the E-sum $_{100}$ FTFC emission lineshape, albeit with a good overall spectral shape for the onset and vibronic tail, is too broad, with an FWHM value that overestimates the experimental value by 0.132 eV. This overestimation is likely due to vibronic contributions, with the vibronic emission spectrum being, on average, overestimated compared to absorption for single snapshots, see Fig.4. The E-sum $_{100}$ FTFC method also produces an overly large Stokes shift value of 0.588 eV, which is 0.254 eV larger than the experimental value, indicating that the overestimation of the emission spectral width may also be due to environmental contributions.

The spectra generated using the more cost-effective E_{opt} -avg₁₀FTFC and E-avg₁₀ZTFC methods are shown in Figure 3c, with the individual components of both approaches shown in Figure 5. Upon optimization of the chromophore, we see that the ensemble of VEE/VDEs narrows, Figure 5 top row, as expected, as thermal energy of the chromophore is removed at the minimum energy geometry within the frozen QM solvent environment. In particular, for the VDEs (top of columns a and b), we see that some of the higher energy transitions at ~ 3.1 - 3.3 eV that were energetically separated from the ensemble are no longer present at these high energies.

We also depict in the middle row of Figure 5 the aver-

age ZTFC and FTFC lineshapes from ten randomly chosen snapshots generated from energetically aligned individual vibronic FC spectra. The optimized VEEs/VDEs and unoptimized VEEs/VDEs, shifted using the average 0-0 transition values from the same snapshots that generate the average FC lineshape, are combined with the average FTFC and ZTFC lineshapes and then summed to produce the E_{opt} -avg₁₀FTFC and E-avg₁₀ZTFC spectra, respectively, shown in the bottom row of Figure 5.

For NBD in DMSO, we see that the absorption spectra generated using all three E-FC approaches are in excellent agreement with each other and with the experimental absorption lineshape. In contrast, the emission spectra from all E-FC methods are broader than experiment. The E_{opt} -avg₁₀FTFC and the E-sum₁₀₀FTFC methods are in impressively good agreement with each other, showing that the use of average FC lineshape can be representative for most snapshots while presenting significant computational savings. The E-avg₁₀ZTFC emission spectrum shows additional over-broadening due to the presence of the high-energy outlier VDEs.

Although the broader emission spectra likely contain contributions from overly strong chromophore-solvent interactions in the excited state, which may contribute to the overestimation of the Stokes shift values, see Table I, they likely also originate from the CAM-B3LYP density functional within the TDA predicting an overly flat excited state potential in explicit QM solvent. This overly flat potential would manifest in both a wider distribution of chromophore configurations sampled during the excited state AIMD and a wider vibronic spectrum, as we see in our average FC lineshapes. This explanation is supported by the much more narrow spectrum generated by a vertical gradient compared to adiabatic Hessian Franck-Condon lineshape (see Figure S7) as well as going beyond the TDA to employing the full TDDFT matrix, which leads to a slight broadening of the absorption spectrum and narrowing of the emission spectrum (see Figure S8). The difference in absorption and emission spectral width also shows some mild dependence on the choice of functional, with LC- ω PBE yielding a more narrow fluorescence spectrum (see Figure S9). In sum, the E-FC methods capture both specific environmental and vibronic effects but are susceptible to errors in the description of the electronic structure, which for NBD in DMSO at the TDA/CAM-B3LYP level of theory appears to yield an overly flat description of the excited state potential.

B. Nile Red in DMSO

Like NBD, NR is also used as a fluorescence emitter^{119,120,135–137} and its spectral properties are sensitive to the environment. ^{123,138} The experimental absorption lineshape is broader than the fluorescence lineshape, with FWHM values of 0.365 eV and 0.252 eV, respectively. ¹²³ Unlike NBD, there are no hydrogen

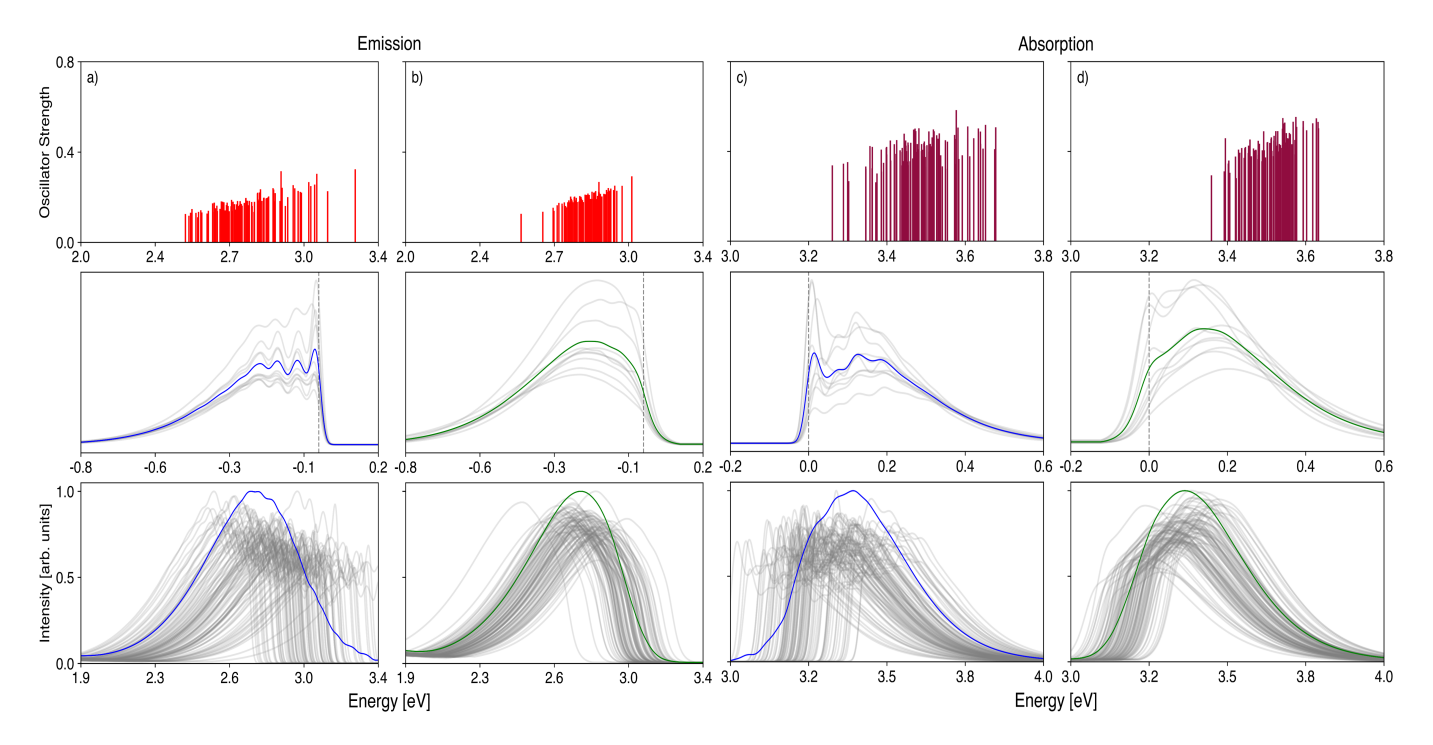


FIG. 5. Pictorial representation of the E-avg₁₀ZTFC and E_{opt} -avg₁₀FTFC methods for NBD in DMSO: The first two columns a) and b) represent emission, and the columns c) and d) represent absorption. The top row shows the distribution of VDEs from a) unoptimized and b) optimized geometries and VEEs from c) unoptimized and d) optimized geometries on the excited and ground state PESs, respectively. The middle row depicts the procedure of generating the average FC lineshape by aligning the $0 \to 0$ transition energies. The bottom row represents the dressing of the ω_{00} shifted unoptimized and optimized VDEs and VEEs with avg₁₀ZTFC and avg₁₀FTFC lineshapes, resulting in E-avg₁₀ZTFC and E_{opt} -avg₁₀FTFC methods, respectively.

bonds between NR and DMSO molecules, and the resulting Stokes shift is noticeably smaller, being 0.290 eV for NR (compared to 0.334 eV for NBD).

From the AIMD simulations, we obtained one hundred uncorrelated snapshots on both the ground and excited state potentials and computed the VEEs and VDEs. For distributions of VEEs and VDEs of NR in the explicit solvent and the solvent contribution of chromophore-only configurations, please refer to figures S10 and S11, respectively.

Fig. 6a shows both absorption and fluorescence line-shapes for NR in DMSO obtained using the standard ensemble and implicit solvent FTFC approaches, with corresponding spectral values given in Table II. For the VEEs and VDEs contributing to the ensemble spectra, the standard deviation is only 0.08 eV due to the rigid structure of NR. The computed FWHM for absorption and emission ensemble spectral lineshapes are 0.210 and 0.179 eV, respectively. These values are underestimated compared to experimental lineshapes, see Table II, which could be due to overly weak interactions of NR in DMSO or due to the missing vibronic contributions. The Stokes shift determined from the ensemble lineshapes is also underestimated at 0.234 eV.

To improve the comparison between the simulated and experimental spectral shape and FWHM, it is necessary to include the missing vibronic contributions. Previ-

TABLE II. NR in DMSO: FWHM, applied energy shift, and Stokes shift from experiment, ensemble, implicit FTFC, and E-FC methods for absorption and emission lineshapes. All values are given in eV.

	Abs	Ems	Abs	Ems	Stokes
Methods	FWHM	FWHM	Energy	Energy	Shift
	(eV)	(eV)	Shift (eV)	Shift (eV)	(eV)
Exp_{LS}	0.365	0.252	-	-	0.290
Implicit	0.114	0.289	1.046	1.323	0.013
Ensemble	0.210	0.179	0.792	0.801	0.234
Ensemble_{Opt}	0.148	0.109	0.788	0.816	0.261
E-avg ₁₀ $ZTFC$	0.300	0.267	0.644	0.788	0.136
E_{opt} -avg ₁₀ FTFC	0.268	0.166	0.627	0.795	0.123
E-sum ₁₀₀ FTFC	0.256	0.228	0.599	0.791	0.098

ous implicit solvent studies by Kostjukova et al. ¹³⁹ and Boldrini et al. ¹⁴⁰ have confirmed the crucial role of vibronic contributions in the absorption spectra of NR. The implicit solvent FTFC simulated absorption and fluorescence spectral lineshapes, see Figure 6a, do not show the smooth spectral lineshapes of the experiment, with FWHM values that are under and over-estimated at 0.114 and 0.289 eV, respectively; both of these values include the second main vibronic peak. The calculated Stokes shift using the corresponding maxima is 0.013 eV, which is severely underestimated due to the small distance between the 0-0 peaks that dominate the lineshape maxima. Thus, we find that both the ensemble and implicit solvent

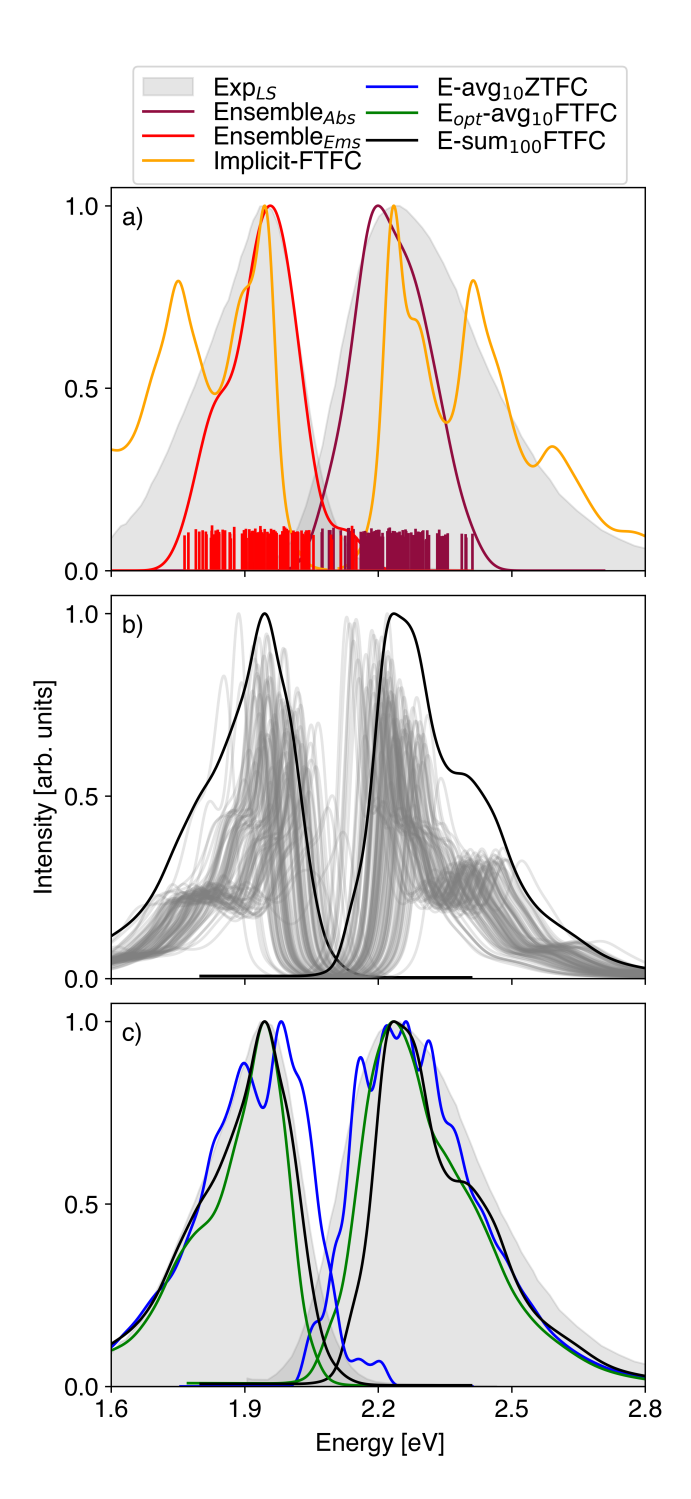


FIG. 6. Absorption and fluorescence lineshapes of NR in DMSO: Filled gray spectra are experimental lineshapes, transformed from Ref. 123. a) Ensemble and implicit solvent FTFC methods, b) E-sum₁₀₀FTFC and individual FTFC spectra, and c) E-avg₁₀ZTFC, E_{opt}-avg₁₀FTFC, and E-sum₁₀₀FTFC lineshapes. All lineshapes are shifted energetically to align with the experimental lineshape maxima.

FTFC methods fail to describe the experimental absorption and emission spectra of NR in DMSO adequately.

Combining an explicit description of the solvent environment with vibronic coupling is essential for an improved description of both absorption and fluorescence spectra.

Next, we compare spectral lineshapes generated with the E-FC methods. The pictorial representation of the working of E-FC methods for NR in DMSO is shown in Figure S12. The individual FTFC spectra and resulting E-sum₁₀₀FTFC lineshape are shown in Fig. 6b. The individual FTFC spectra computed in the explicit solvent environment are quite similar to each other across configurations and they do not show the same intensity in the second vibronic peak as is seen with the implicit solvent FTFC spectra. The FWHM values for the individual spectra do not usually account for the contributions from the second vibronic peak, leading to very small values. Therefore, in Figure 7, we instead plot the fullwidth half-half max (FWHHM), taking the width at 25% of the lineshape maximum. At 25% of the maximum, we observe broadening primarily from two vibronic peaks in both absorption and emission lines. However, there are some single-peak outliers in both FWHHM distributions. For absorption, widths below 0.20 eV originate from a single peak, which in Figure 7a we represent by light blue bars. For emission, widths below 0.20 eV are due to a combination of both single and double peaks; in Figure 7b, these values are colored light blue with gray stripes. We computed the average value of this FWHHM using only the spectra for which there are two vibronic peaks contributing to the FWHHM value, which we determined to be 0.274 for absorption and 0.264 eV for fluorescence. These values are smaller than the corresponding implicit solvent FWHHM values of 0.452 and 0.470 eV taken at the 25% intensity value, showing decreased vibronic coupling in explicit solvent. The summation of the E-sum₁₀₀FTFC method washes out the pronounced vibronic nature of the peaks, providing relatively smooth absorption and fluorescence lineshapes, as observed in the experimental lineshapes.

The E_{opt} -avg₁₀FTFC and E-avg₁₀ZTFC spectra are shown in Fig. 6c. In contrast to the NBD results, for NR, the E-sum₁₀₀FTFC and E_{opt} -avg₁₀FTFC fluorescence spectra agree in width and shape with the experiment, whereas the absorption spectrum is predicted to be too narrow by both methods. For the E-avg₁₀ZTFC method, the lineshapes remain a bit jagged, and there is an increase in lineshape width, leading to an overly broad fluorescence lineshape. We also see for fluorescence that there are clearly a few high-energy outlier VDEs that lead to an unphysical high-energy fluorescence spectral onset. The Stokes shift predicted by all three methods, see Table II, remains underestimated compared to the experiment. Overall, the more affordable E_{opt} avg₁₀FTFC method is again in good agreement with the E-sum₁₀₀FTFC method, with the E-avg₁₀ZTFC showing more of a discrepancy with some unphysical jaggedness remaining in the spectrum.

The electronic structure method is undoubtedly one source of potential error for the missing spectral width

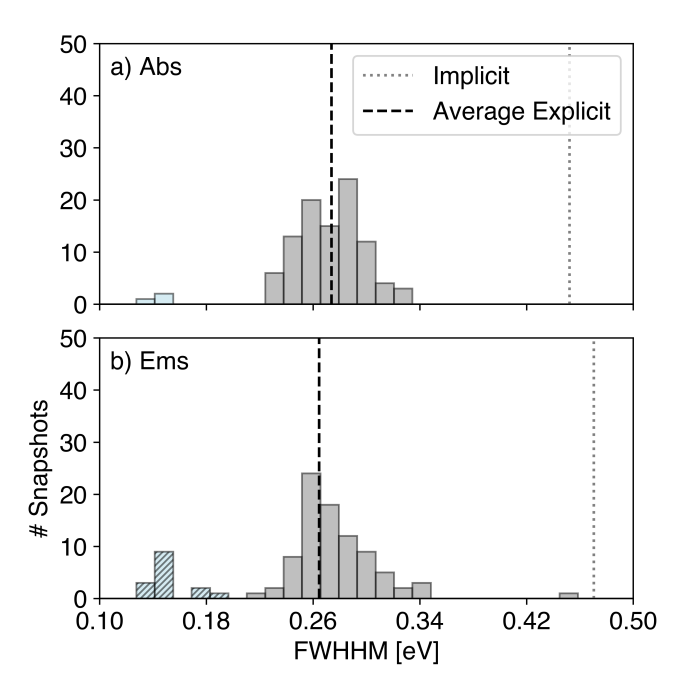


FIG. 7. Frequency distribution of a) absorption and b) emission vibronic lineshape widths computed at 25% intensity, Full Width at Half-Half Maximum (FWHHM), of NR in DMSO. The dotted gray lines correspond to the FWHHM value of the implicit solvent FTFC spectra (Abs: 0.452 eV, Ems: 0.470 eV), which includes the second main vibronic peak. The dashed black lines represent the average values of the FWHHM of the explicit solvent FTFC spectra that include the second main vibronic peak (Abs: 0.274 eV, Ems: 0.264 eV).

for NR in DMSO. When we examined the effect of the TDA versus the full solution of the TDDFT equations on five snapshots, we found that the second vibronic peak gains significant intensity in both absorption and emission spectra (see Figure S13), which would lead to a considerable broadening of the simulated absorption and emission spectra if the TDDFT lineshape was used instead of the TDA lineshape. Additionally, benchmarking FTFC lineshapes against two other density functionals showed that although the M06-2X method gives good agreement with the CAM-B3LYP lineshapes, the LC- ω HPBE functional produces FTFC spectra that are substantially broader than the other two functionals (Figure S14). Thus, by changing the electronic structure method to one with broader vibronic spectra, we can expect improved agreement with the experimental absorption spectrum; however, the emission spectrum would also gain additional broadening and become broader than the experimental spectrum. Overall, the vibronic broadening appears underestimated with TDA-CAM-B3LYP for Nile Red in DMSO. This underestimated vibronic broadening may also be responsible for the underestimated Stokes shifts, as the increased intensity of the second vibronic peak may change the position of the spectral maxima and increase the energy between the maxima of the absorp-

TABLE III. 7MC in methanol: FWHM, applied energy shift, and Stokes shift from experiment, ensemble, implicit FTFC, and E-FC methods for absorption and emission lineshapes. All values are given in eV.

Methods	Abs FWHM (eV)	Ems FWHM (eV)	Abs Energy Shift (eV)	Ems Energy Shift (eV)	Stokes Shift (eV)
Exp_{LS}	0.563	0.539	-	-	0.683
Implicit	0.539	0.766	0.303	0.380	0.602
Ensemble	0.203	0.445	0.587	0.478	0.673
Ensemble_{Opt}	0.229	0.235	0.642	0.722	0.582
E-avg ₁₀ ZTFC	0.494	0.779	0.444	0.646	0.464
E_{opt} -avg ₁₀ FTFC	0.490	0.653	0.412	0.604	0.484
E-sum ₁₀₀ FTFC	0.480	0.585	0.468	0.605	0.546

tion and emission spectra.

C. 7MC in Methanol

7-Methoxycoumarin-4-acetic acid (7MC), like NBD, is a push-pull electron system and is used as a fluorescent probe in various cell biology applications. ^{121,122,141} 7MC shows the largest conformational changes and the largest number of hydrogen bonds of all three dyes studied here. Due to the carboxylic acid group and the carbonyl bond, 7MC acts as both an acceptor and donor of hydrogen bonds in methanol. The experimental FWHM values are 0.563 and 0.539 eV for absorption and emission lineshapes, indicating similar potential energy surfaces for ground and excited states with a Stokes shift of 0.683 eV, the largest among all three dyes studied here.

Like the other two dyes, we extracted 100 snapshots from the ground and excited state AIMD simulations and performed VEE and VDE calculations. See Figures S15 and S16 for trends in VEEs and VDEs in both explicit solvent and chromophore-only configurations.

Upon analyzing the geometrical changes throughout the dynamics, we observed a considerable increase in the flexibility in the excited state, particularly around the pyrone ring. Consequently, the value of the standard deviation of the energy gap distribution more than doubles, going from 0.119 eV for VEEs to 0.285 eV for VDEs, see Table S3. However, once the geometries are optimized in frozen QM solvent, the standard deviation values decrease to 0.077 and 0.097, respectively.

Figure 8a shows lineshapes generated using the ensemble and implicit solvent FTFC approaches. Although the ensemble absorption spectral lineshape is too narrow compared to the experiment, the ensemble emission lineshape is twice as broad as absorption, nearing the experimental spectral width and giving a FWHM value of 0.445 eV, see Table III. The difference in absorption and emission spectral width correlates to the standard deviation computed for the VEEs and VDEs.

The implicit FTFC absorption lineshape displays distinct vibronic peaks, whereas the emission lineshape appears smoother and broader. The FTFC computed FWHM values are $0.539~{\rm eV}$ and $0.766~{\rm eV}$, respectively,

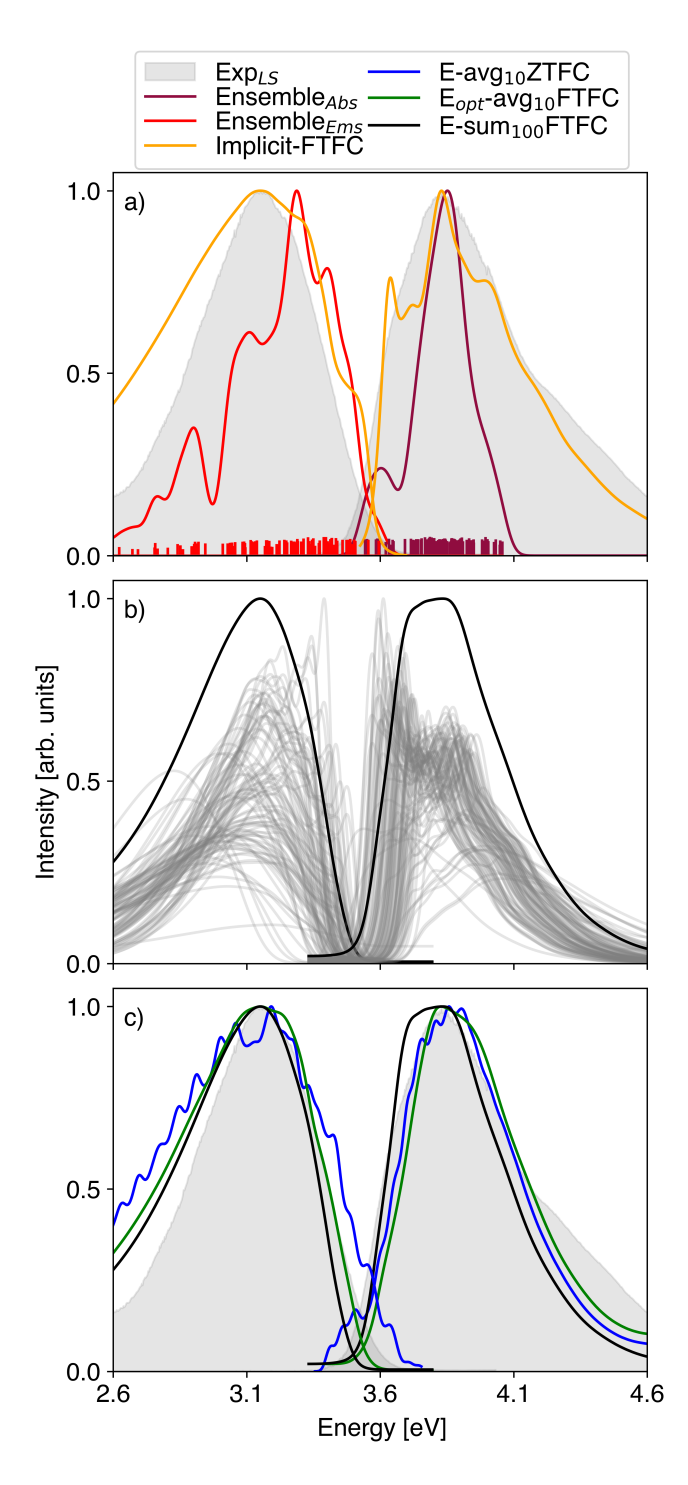


FIG. 8. Absorption and fluorescence lineshapes of 7MC in methanol: Filled gray spectra are experimental lineshapes, transformed from Ref. 124,125. a) Ensemble and implicit solvent FTFC methods, b) E-sum₁₀₀FTFC and individual FTFC spectra, and c) E-avg₁₀ZTFC, E_{opt}-avg₁₀FTFC, and E-sum₁₀₀FTFC lineshapes. All lineshapes are shifted energetically to align with the experimental lineshape maxima.

with a Stokes shift of 0.602 eV. Thus, similar to NBD, both the ensemble and the implicit solvent FTFC ap-

proaches predict a wider emission spectral lineshape than absorption, contrary to the experiment, suggesting an overly flat excited state potential at this level of theory.

Next, we compare the spectra generated with the E-FC family of approaches. The pictorial representation of the working of E-FC methods for 7MC in methanol is shown in Figure S17. The individual explicit solvent FTFC absorption and fluorescence lineshapes of 7MC in methanol, along with the resulting E-sum₁₀₀FTFC spectra, are shown in Figure 8b. We find that there is a large degree of variability in the features of the individual FTFC lineshapes, but the trend of the FWHM values is consistent with the wider emission predicted by implicit solvent, with average values of 0.416 eV for the absorption lineshape and 0.630 eV for the emission lineshape, see FWHM distribution in Figure 9. Both of these values are smaller than those predicted by the implicit solvent approach, suggesting that for 7MC, the explicit solvent decreases the vibronic coupling compared to the implicit solvent model, opposite of what we see with NBD. The relatively broader implicit solvent FTFC lineshapes are due to the larger displacement of the excited state potentials in implicit solvent, leading to more vibronic broadening.

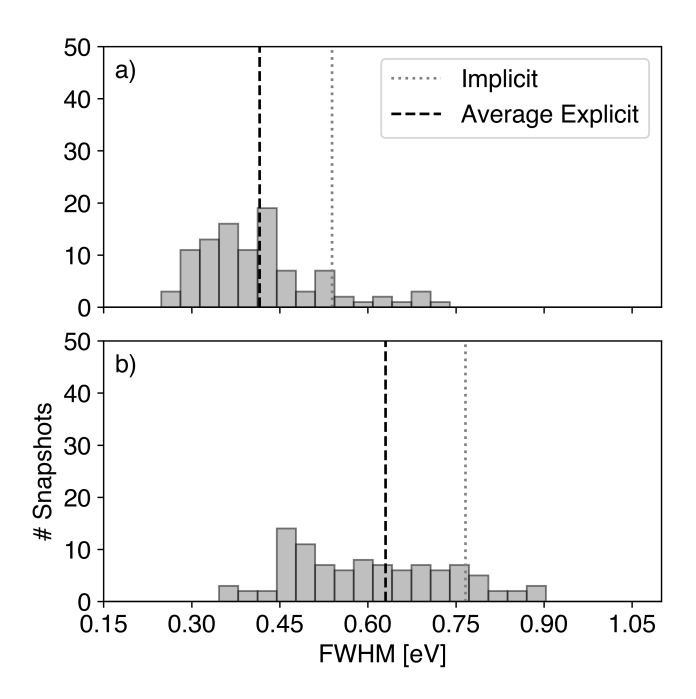


FIG. 9. Frequency distribution of a) absorption and b) emission vibronic lineshape FWHM values of 7MC in methanol. The dotted gray lines correspond to the FWHM of the implicit solvent FTFC spectra (Abs: 0.539 eV, Ems: 0.766 eV). The dashed black lines represent the average values of the FWHM of the explicit solvent FTFC spectra (Abs: 0.416 and Ems: 0.630 eV).

Although it is difficult to separate the role of individual factors affecting the lineshape, our analysis suggests that the most important geometrical change is associated with the planarity of the pyrone ring. For spectra with no vibronic features, the ring remains out-of-plane after optimization. For emission, we observe three distinct categories: spectra with the first peak as the maximum, spectra with the second peak as the maximum, and only one maximum but overly broad. Following the same procedure as with the other dyes, we chose random snapshots for generating the average FC lineshape, and found that there is minimal variation after ten vibronic spectra are included in the averaging procedure. Given the variability of lineshapes, a more sophisticated averaging scheme could be envisioned that weights the lineshape based on the percentage of particular configurations, but here, we choose not to explore this direction.

Figure 8c compares the absorption and emission lineshapes generated using the three E-FC methods. All three methods show good agreement for the absorption lineshape and similar FWHM ($\sim 0.490 \text{ eV}$) but remain underestimated in width relative to the experiment. For the emission lineshapes, both E_{opt} -avg₁₀FTFC and E-sum₁₀₀FTFC show good agreement with each other, with E-sum₁₀₀FTFC producing a more narrow spectrum (FWHM is 0.585 eV for E-sum₁₀₀FTFC, 0.653 eV for E_{opt} -avg₁₀FTFC), whereas the emission spectrum of the E-avg₁₀ZTFC method is wider and jagged because of the large distribution of VDEs, leading to an overly large FWHM value of 0.779 eV. Unlike NBD, this overly large broadening appears to be completely dominated by chromophore flexibility. About 33% of emission lineshapes have an FWHM of more than 0.7 eV, and these are the snapshots where the pyrone ring is no longer planar. As shown in Table III, the predicted Stokes shift is underestimated by all three methods.

Unlike the other two chromophores, the 7MC spectral lineshape differences from full TD-DFT and TDA are minimal for both absorption and emission, as shown in Figure S18. Compared to CAM-B3LYP, both M06-2X, and LC- ω HPBE predict broader lineshapes for absorption and slightly broader FTFC spectra for emission, as shown in Figure S19. This comparison suggests that CAM-B3LYP may underestimate the vibronic progression for absorption, leading to a more narrow absorption lineshape. As the wide distribution of VDEs suggests a potentially flat and anharmonic excited state S₁ surface, we also compared our vibronic lineshape computed with the adiabatic Hessian approach, the lineshape generated with the vertical gradient and adiabatic shift approaches, finding that for planar configurations there is good agreement between methods, whereas for more bent chromophore configurations the adiabatic Hessian produces a broader lineshape, see SM, Figure S20. This broader lineshape supports that the excited state potential is indeed anharmonic at this geometry for this flexible degree of freedom, leading to a breakdown of the harmonic approximation and contributions from overly broad lineshape within the adiabatic Hessian approach.

Ultimately, we see similar trends for E-FC approaches with 7MC as with the other dyes, where E-sum $_{100}{\rm FTFC}$

and E_{opt} -avg₁₀FTFC are in good agreement, but E-avg₁₀ZTFC is generally too broad and jagged with the $135~{\rm cm}^{-1}$ broadening factor used here.

D. Relative Computational Cost of E-FC Methods

We next show the computational cost associated with the various ensemble and E-FC spectroscopy methods, accounting for the electronic structure calculations on the MD snapshots. We do not consider the computational cost from the QM/MM AIMD sampling, which is substantial, and could be accelerated with recent approaches of machine learning interatomic potentials. 142-147. The chart depicted in Figure 10 illustrates the relative computational wall time required for the various spectroscopy methods, with average results given for simulating absorption. See Figure S21 for the corresponding relative costs for emission, which is similar but has an increased computational cost for excited state geometry optimization for the E_{opt} approach. Relative times are averaged over the three dyes investigated in this study. The geometry optimization and excitation energies were performed using TeraChem on a dual NVIDIA Tesla A100 PCIe v4 40GB HBM2 Passive Single GPU setup. Frequency calculations for the ground and excited states of NBD in DMSO, as well as 7MC in methanol, were carried out utilizing Gaussian 16 on two Intel 28-core Xeon Gold 6330 processors, equipped with 256GB and 1TB of RAM, respectively, with the latter configuration used for the NR dye in DMSO.

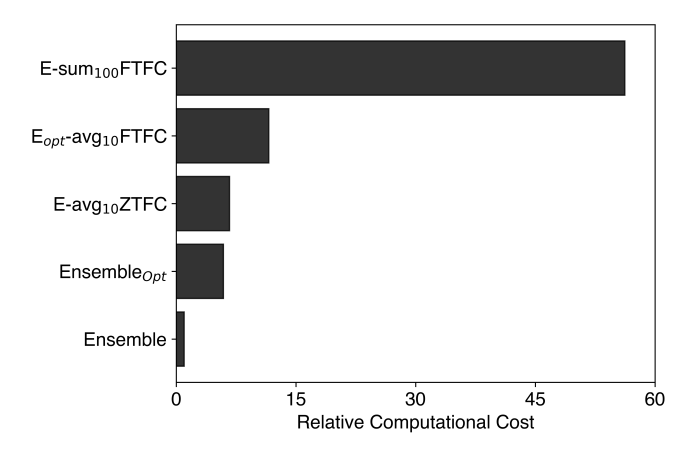


FIG. 10. The average relative computational cost of all explicit solvent absorption spectroscopy methods for all three dyes.

The E-sum₁₀₀FTFC method is by far the most computationally demanding, taking $56.2\times$ as long as the ensemble approach alone. Note that due to the larger QM region size for NR in DMSO, the frequency calculations are more computationally expensive, leading to a larger relative cost for the E-sum₁₀₀FTFC approach. There is a substantial reduction in computational cost achieved

through the use of more approximate methods, with the E_{opt} -avg₁₀FTFC method taking only $11.6\times$ and the E-avg₁₀ZTFC method taking only $6.7\times$ as long as the ensemble approach. For the E_{opt} -avg₁₀FTFC approach, this decrease in computational cost comes with nearly the same accuracy as the E-sum₁₀₀FTFC method, underscoring the efficiency of this approach and making it our recommended E-FC method for spectroscopic simulations.

V. CONCLUSIONS

In this study, we compared the simulated absorption and fluorescence lineshapes computed with three combined ensemble-Franck-Condon methods that account for both explicit environmental effects and vibronic effects. The explicit solvent is modeled through QM/MM AIMD trajectories performed on the ground state and the excited state. The vibronic effects are captured through the simulation of Franck-Condon spectra for the chromophore embedded in a frozen QM solvent shell. These E-FC methods are used to generate spectral lineshapes for three different chromophore-solvent systems and are compared to the more standard ensemble and implicit solvent Franck-Condon approaches.

We find that for both absorption and fluorescence, the E_{opt} -avg₁₀FTFC approach matches very well with the more expensive E-sum₁₀₀FTFC approach, generating very similar spectra at approximately 25% of the computational cost, and this, therefore, is our recommended approach for capturing vibronic and environmental effects for spectral lineshapes. The main approximation of the E_{opt} -avg₁₀FTFC approach is the assumption of an average FTFC lineshape, which we find here works very well with an average over ten individual lineshapes generated in explicit QM solvent. The E-avg₁₀ZTFC approach shows some over-broadening due to outliers from the MD sampling and jaggedness in the spectra but presents a reasonable alternative for 12.5% of the computational cost of the E-sumFTFC method.

One way to assess the extent of vibronic coupling is by measuring the width of the spectra before accounting for environmental broadening. Compared to FTFC spectra computed with implicit solvent, the FTFC spectra computed in explicit solvent showed stronger vibronic coupling (larger average FWHM) for NBD but weaker vibronic coupling for NR and 7MC. Errors in the simulated lineshape FWHM values can be traced to the underlying electronic structure methods and the extent of vibronic coupling for each method. We find here that the choice of density functional theory affects the lineshape, with more exact exchange tending to lead to stronger vibronic coupling and broader spectra NR but slightly weaker coupling for NBD. We also find that the use of the TDA, compared to full TDDFT, can lead to more narrow vibronic spectral lineshapes in some cases.

Our study of computed absorption and emission line-

shapes showcases the ability of a variety of spectroscopy simulation methods to capture vibronic and environmental effects. Advances in computational power, particularly GPUs, now allow ground and excited state explicit solvent interactions and vibronic contributions to be incorporated into molecules' absorption and fluorescence spectra, paving the way for accurate simulations of full spectral lineshapes. However, many challenges remain, including determining an accurate level of electronic structure theory and incorporating nonadiabatic and nuclear quantum effects. Many efforts along these fronts are underway, broadening the ability of simulation to connect with complex spectroscopic experiments.

VI. SUPPLEMENTARY MATERIAL

The Supplementary Material is available free of charge and provided with the article. It contains information on MD and AIMD simulation setup, FC lineshape averaging procedure, experimental spectra transformation to wavenumbers and lineshapes, and unshifted spectral lineshapes of all dyes. For each dye, there are graphs showing VEEs and VDEs across snapshots, pictorial representation of E-FC methods for NR and 7MC, graphs comparing full TDDFT and TDA, as well as DFT functional comparison for vibronic lineshapes.

VII. ACKNOWLEDGEMENTS

This work was supported by NSF Grant No. CHE-1955656. This research used computing resources of the MERCED cluster at UC Merced under NSF Grant No. 1429783 and the Pinnacles cluster at UC Merced under NSF Grant No. 2019144. A. K. would like to express his sincerest gratitude to Dr. Anne Myers Kelley for her assistance and guidance.

VIII. DATA AVAILABILITY

The dataset used to support the article's findings can be downloaded from the Harvard Dataverse, https://doi.org/10.7910/DVN/H1YGKX, under the CC0 1.0 license. This dataset contains AIMD simulation files, optimized geometries, frequency calculations, and Franck-Condon spectra of all three dyes reported in the article. However, due to the large size of the molecular dynamics trajectories and Gaussian checkpoint files, they are not included in the repository and instead are available on request.

IX. REFERENCES

¹J. Franck and E. G. Dymond, "Elementary processes of photochemical reactions," Transactions of the Faraday Society **21**, 536 (1926).

- ²E. Condon, "A theory of intensity distribution in band systems," Physical Review **28**, 1182–1201 (1926).
- ³P. T. Ruhoff and M. A. Ratner, "Algorithms for computing franck-condon overlap integrals," International Journal of Quantum Chemistry 77, 383–392 (2000).
- ⁴J. R. Reimers, "A practical method for the use of curvilinear coordinates in calculations of normal-mode-projected displacements and duschinsky rotation matrices for large molecules," The Journal of Chemical Physics 115, 9103-9109 (2001).
- ⁵A. Toniolo and M. Persico, "Efficient calculation of franck-condon factors and vibronic couplings in polyatomics," Journal of Computational Chemistry 22, 968–975 (2001).
- ⁶T. Petrenko and F. Neese, "Analysis and prediction of absorption band shapes, fluorescence band shapes, resonance raman intensities, and excitation profiles using the time-dependent theory of electronic spectroscopy," The Journal of Chemical Physics 127, 164319 (2007).
- ⁷F. Santoro, R. Improta, A. Lami, J. Bloino, and V. Barone, "Effective method to compute franck-condon integrals for optical spectra of large molecules in solution," The Journal of Chemical Physics 126, 084509 (2007).
- ⁸V. Barone, J. Bloino, M. Biczysko, and F. Santoro, "Fully integrated approach to compute vibrationally resolved optical spectra: From small molecules to macrosystems," Journal of Chemical Theory and Computation 5, 540–554 (2009).
- ⁹J. Bloino, M. Biczysko, F. Santoro, and V. Barone, "General approach to compute vibrationally resolved one-photon electronic spectra," Journal of Chemical Theory and Computation 6, 1256–1274 (2010).
- ¹⁰T. Petrenko and F. Neese, "Efficient and automatic calculation of optical band shapes and resonance raman spectra for larger molecules within the independent mode displaced harmonic oscillator model," The Journal of Chemical Physics 137, 234107 (2012).
- ¹¹D. W. Silverstein and L. Jensen, "Vibronic coupling simulations for linear and nonlinear optical processes: Theory," The Journal of Chemical Physics 136, 064111 (2012).
- ¹²F. J. A. Ferrer and F. Santoro, "Comparison of vertical and adiabatic harmonic approaches for the calculation of the vibrational structure of electronic spectra," Physical Chemistry Chemical Physics 14, 13549 (2012).
- ¹³ A. Baiardi, J. Bloino, and V. Barone, "General time dependent approach to vibronic spectroscopy including franck-condon, herzberg-teller, and duschinsky effects," Journal of Chemical Theory and Computation 9, 4097–4115 (2013).
- ¹⁴A. Baiardi, J. Bloino, and V. Barone, "General formulation of vibronic spectroscopy in internal coordinates," The Journal of Chemical Physics 144, 084114 (2016).
- ¹⁵B. de Souza, F. Neese, and R. Izsák, "On the theoretical prediction of fluorescence rates from first principles using the path integral approach," The Journal of Chemical Physics 148, 034104 (2018)
- ¹⁶D. Madsen, O. Christiansen, P. Norman, and C. König, "Vibrationally resolved emission spectra of luminescent conjugated oligothiophenes from anharmonic calculations," Physical Chemistry Chemical Physics 21, 17410–17422 (2019).
- ¹⁷R. Gherib, S. N. Genin, and I. G. Ryabinkin, "On the importance of well-defined thermal correlation functions in simulating vibronic spectra," The Journal of Physical Chemistry A 126, 3947–3956 (2022).
- ¹⁸F. Santoro, A. Lami, R. Improta, and V. Barone, "Effective method to compute vibrationally resolved optical spectra of large molecules at finite temperature in the gas phase and in solution," The Journal of Chemical Physics 126 (2007), 10.1063/1.2721539.
- ¹⁹E. Tapavicza, F. Furche, and D. Sundholm, "Importance of vibronic effects in the uvvis spectrum of the 7, 7, 8, 8-tetracyanoquinodimethane anion," Journal of Chemical Theory and Computation 12, 50585066 (2016).

- ²⁰S. Miertus, E. Scrocco, and J. Tomasi, "Electrostatic interaction of a solute with a continuum. a direct utilizaion of AB initio molecular potentials for the prevision of solvent effects," Chemical Physics 55, 117–129 (1981).
- ²¹S. Miertus and J. Tomasi, "Approximate evaluations of the electrostatic free energy and internal energy changes in solution processes," Chemical Physics 65, 239–245 (1982).
- ²²J. L. Pascual-ahuir, E. Silla, and I. Tuñon, "GEPOL: An improved description of molecular surfaces. III. a new algorithm for the computation of a solvent-excluding surface," Journal of Computational Chemistry 15, 1127–1138 (1994).
- ²³E. Cances, B. Mennucci, and J. Tomasi, "A new integral equation formalism for the polarizable continuum model: Theoretical background and applications to isotropic and anisotropic dielectrics," The Journal of Chemical Physics 107, 3032–3041 (1997).
- ²⁴R. Cammi, "Coupled-cluster theories for the polarizable continuum model. II. analytical gradients for excited states of molecular solutes by the equation of motion coupled-cluster method," International Journal of Quantum Chemistry 110, 3040–3052 (2010).
- ²⁵V. Barone and M. Cossi, "Quantum calculation of molecular energies and energy gradients in solution by a conductor solvent model," The Journal of Physical Chemistry A 102, 1995–2001 (1998).
- ²⁶J. M. Herbert, "Dielectric continuum methods for quantum chemistry," WIREs Computational Molecular Science 11 (2021), 10.1002/wcms.1519.
- ²⁷J. Cerezo, F. J. A. Ferrer, G. Prampolini, and F. Santoro, "Modeling solvent broadening on the vibronic spectra of a series of coumarin dyes. from implicit to explicit solvent models," Journal of Chemical Theory and Computation 11, 5810–5825 (2015).
- ²⁸T. J. Zuehlsdorff and C. M. Isborn, "Combining the ensemble and franck-condon approaches for calculating spectral shapes of molecules in solution," The Journal of Chemical Physics 148, 024110 (2018).
- ²⁹ J. P. Bergsma, P. H. Berens, K. R. Wilson, D. R. Fredkin, and E. J. Heller, "Electronic spectra from molecular dynamics: a simple approach," The Journal of Physical Chemistry 88, 612– 619 (1984), https://doi.org/10.1021/j150647a055.
- ³⁰ J. R. Reimers, K. R. Wilson, and E. J. Heller, "Complex time-dependent wave packet technique for thermal equilibrium systems: Electronic spectra," J. Chem. Phys. **79**, 4749–4757 (1983).
- ³¹R. Crespo-Otero and M. Barbatti, "Spectrum simulation and decomposition with nuclear ensemble: formal derivation and application to benzene, furan and 2-phenylfuran," Theoretical Chemistry Accounts 131 (2012), 10.1007/s00214-012-1237-4.
- ³²L. I. T. S. L. F. R. da S. Junior Luiz Antonio Ribeiro de Sousa Junior Rafael Timoteo and da Silva Filho Demetrio A., "A dft study of a set of natural dyes for organic electronics," Journal of Molecular Modeling 23, 343 (2017).
- ³³F. Kossoski and M. Barbatti, "Nuclear ensemble approach with importance sampling," Journal of Chemical Theory and Computation 14, 3173–3183 (2018).
- ³⁴W. Zeng, S. Gong, C. Zhong, and C. Yang, "Prediction of oscillator strength and transition dipole moments with the nuclear ensemble approach for thermally activated delayed fluorescence emitters," The Journal of Physical Chemistry C 123, 1008110086 (2019).
- 35. "Sre, D. Hollas, and P. Slavek, "Uv absorption of criegee intermediates: quantitative cross sections from high-level ab initio theory," Physical Chemistry Chemical Physics 20, 64216430 (2018).
- ³⁶. "Sre, J. Sita, P. Slavek, V. Ladnyi, and D. Heger, "Limits of the nuclear ensemble method for electronic spectra simulations: Temperature dependence of the (e)-azobenzene spectrum," Journal of Chemical Theory and Computation 16, 64286438 (2020).

- ³⁷. "Sre and P. Slavek, "Optimal representation of the nuclear ensemble: Application to electronic spectroscopy," Journal of Chemical Theory and Computation 17, 63956404 (2021).
- ³⁸ A. "Prlj, E. Marsili, L. Hutton, D. Hollas, D. Shchepanovska, D. R. Glowacki, P. Slavek, and B. F. E. Curchod, "Calculating photoabsorption cross-sections for atmospheric volatile organic compounds," ACS Earth and Space Chemistry 6, 207217 (2021).
- ³⁹V. Barone, J. Bloino, S. Monti, A. Pedone, and G. Prampolini, "Fluorescence spectra of organic dyes in solution: a time dependent multilevel approach," Phys. Chem. Chem. Phys. 13, 21602166 (2011).
- ⁴⁰A. Petrone, J. Cerezo, F. J. A. Ferrer, G. Donati, R. Improta, N. Rega, and F. Santoro, "Absorption and emission spectral shapes of a prototype dye in water by combining classical/dynamical and quantum/static approaches," The Journal of Physical Chemistry A 119, 5426–5438 (2015), pMID: 25699575, https://doi.org/10.1021/jp510838m.
- ⁴¹S. Skoko, C. Micheletti, E. Grifoni, F. Egidi, T. Giovannini, A. Pucci, and C. Cappelli, "Towards a cost-effective modeling of fluorescence in the condensed phase," Dyes and Pigments 215, 111227 (2023).
- ⁴²R. Youngworth and B. Roux, "Simulating the fluorescence of di-8-anepps in solvents of different polarity," The Journal of Physical Chemistry B 128, 184192 (2023).
- ⁴³R. Youngworth and B. Roux, "Simulating the fluorescence of the locally excited state of dmabn in solvents of different polarities," The Journal of Physical Chemistry B 128, 172183 (2023).
- ⁴⁴D. Gegiou, K. A. Muszkat, and E. Fischer, "Temperature dependence of photoisomerization. VI. viscosity effect," Journal of the American Chemical Society 90, 12–18 (1968).
- ⁴⁵B.-X. Xue, M. Barbatti, and P. O. Dral, "Machine learning for absorption cross sections," The Journal of Physical Chemistry A 124, 7199–7210 (2020).
- ⁴⁶S. Mukamel, Principles of Nonlinear Optical Spectroscopy (Oxford University Press, New York, 1995).
- ⁴⁷M. C. Zwier, J. M. Shorb, and B. P. Krueger, "Hybrid molecular dynamics-quantum mechanics simulations of solute spectral properties in the condensed phase: Evaluation of simulation parameters," Journal of Computational Chemistry 28, 15721581 (2007).
- ⁴⁸A. M. Rosnik and C. Curutchet, "Theoretical characterization of the spectral density of the water-soluble chlorophyll-binding protein from combined quantum mechanics/molecular mechanics molecular dynamics simulations," Journal of Chemical Theory and Computation 11, 58265837 (2015).
- ⁴⁹S. Chandrasekaran, M. Aghtar, S. Valleau, A. Aspuru-Guzik, and U. Kleinekathöfer, "Influence of force fields and quantum chemistry approach on spectral densities of bchl a in solution and in fmo proteins," The Journal of Physical Chemistry B 119, 999510004 (2015).
- ⁵⁰M. K. Lee, P. Huo, and D. F. Coker, "Semiclassical path integral dynamics: Photosynthetic energy transfer with realistic environment interactions," Annual Review of Physical Chemistry 67, 639668 (2016).
- ⁵¹D. Loco and L. Cupellini, "Modeling the absorption lineshape of embedded systems from molecular dynamics: A tutorial review," International Journal of Quantum Chemistry 119 (2018), 10.1002/qua.25726.
- ⁵²D. Loco, S. Jurinovich, L. Cupellini, M. F. S. J. Menger, and B. Mennucci, "The modeling of the absorption lineshape for embedded molecules through a polarizable QM/MM approach," Photochem. Photobiol. Sci. 17, 552–560 (2018).
- ⁵³F. Segatta, L. Cupellini, M. Garavelli, and B. Mennucci, "Quantum chemical modeling of the photoinduced activity of multichromophoric biosystems: Focus review," Chemical Reviews 119, 93619380 (2019).
- ⁵⁴T. J. Zuehlsdorff, H. Hong, L. Shi, and C. M. Isborn, "Influence of electronic polarization on the spectral density," The Journal of Physical Chemistry B **124**, 531543 (2019).

- ⁵⁵T. J. Zuehlsdorff, H. Hong, L. Shi, and C. M. Isborn, "Nonlinear spectroscopy in the condensed phase: The role of duschinsky rotations and third order cumulant contributions," The Journal of Chemical Physics 153 (2020), 10.1063/5.0013739.
- ⁵⁶M. Bondanza, L. Cupellini, F. Lipparini, and B. Mennucci, "The multiple roles of the protein in the photoactivation of orange carotenoid protein," Chem 6, 187203 (2020).
- ⁵⁷T. J. Zuehlsdorff, S. V. Shedge, S.-Y. Lu, H. Hong, V. P. Aguirre, L. Shi, and C. M. Isborn, "Vibronic and environmental effects in simulations of optical spectroscopy," Annual Review of Physical Chemistry 72, 165188 (2021).
- ⁵⁸M. S. Chen, Y. Mao, A. Snider, P. Gupta, A. Montoya-Castillo, T. J. Zuehlsdorff, C. M. Isborn, and T. E. Markland, "Elucidating the role of hydrogen bonding in the optical spectroscopy of the solvated green fluorescent protein chromophore: Using machine learning to establish the importance of high-level electronic structure," The Journal of Physical Chemistry Letters 14, 66106619 (2023).
- ⁵⁹S. Del Galdo, M. Fus, and V. Barone, "The oniom/pmm model for effective yet accurate simulation of optical and chiroptical spectra in solution: Camphorquinone in methanol as a case study," Journal of Chemical Theory and Computation 16, 32943306 (2020).
- ⁶⁰G. Mancini, S. Del Galdo, B. Chandramouli, M. Pagliai, and V. Barone, "Computational spectroscopy in solution by integration of variational and perturbative approaches on top of clusterized molecular dynamics," Journal of Chemical Theory and Computation 16, 57475761 (2020).
- ⁶¹E. Falbo, M. Fus, F. Lazzari, G. Mancini, and V. Barone, "Integration of quantum chemistry, statistical mechanics, and artificial intelligence for computational spectroscopy: The uvvis spectrum of tempo radical in different solvents," Journal of Chemical Theory and Computation 18, 62036216 (2022).
- ⁶²J. Cerezo, D. Aranda, F. J. Avila Ferrer, G. Prampolini, and F. Santoro, "Adiabatic-molecular dynamics generalized vertical hessian approach: A mixed quantum classical method to compute electronic spectra of flexible molecules in the condensed phase," Journal of Chemical Theory and Computation 16, 1215–1231 (2020), pMID: 31855424, https://doi.org/10.1021/acs.jctc.9b01009.
- ⁶³A. Segalina, J. Cerezo, G. Prampolini, F. Santoro, and M. Pastore, "Accounting for vibronic features through a mixed quantum-classical scheme: Structure, dynamics, and absorption spectra of a perylene diimide dye in solution," Journal of Chemical Theory and Computation 16, 7061–7077 (2020), pMID: 33124412, https://doi.org/10.1021/acs.jctc.0c00919.
- ⁶⁴T. J. Zuehlsdorff and C. M. Isborn, "Modeling absorption spectra of molecules in solution," International Journal of Quantum Chemistry 119 (2018), 10.1002/qua.25719.
- ⁶⁵T. J. Zuehlsdorff, A. Montoya-Castillo, J. A. Napoli, T. E. Markland, and C. M. Isborn, "Optical spectra in the condensed phase: Capturing anharmonic and vibronic features using dynamic and static approaches," The Journal of Chemical Physics 151, 074111 (2019).
- ⁶⁶S. V. Shedge, T. J. Zuehlsdorff, M. J. Servis, A. E. Clark, and C. M. Isborn, "Effect of ions on the optical absorption spectra of aqueously solvated chromophores," The Journal of Physical Chemistry A 123, 6175–6184 (2019).
- ⁶⁷S. V. Shedge, T. J. Zuehlsdorff, A. Khanna, S. Conley, and C. M. Isborn, "Explicit environmental and vibronic effects in simulations of linear and nonlinear optical spectroscopy," The Journal of Chemical Physics 154, 084116 (2021).
- ⁶⁸J. A. Bjorgaard, K. A. Velizhanin, and S. Tretiak, "Nonequilibrium solvent effects in born-oppenheimer molecular dynamics for ground and excited electronic states," The Journal of Chemical Physics 144 (2016), 10.1063/1.4946009.
- ⁶⁹T. Nelson, S. Fernandez-Alberti, A. E. Roitberg, and S. Tretiak, "Nonadiabatic excited-state molecular dynamics: Modeling photophysics in organic conjugated materials," Accounts of Chemical Research 47, 11551164 (2014).

- ⁷⁰F. J. Avila Ferrer, J. Cerezo, E. Stendardo, R. Improta, and F. Santoro, "Insights for an accurate comparison of computational data to experimental absorption and emission spectra: Beyond the vertical transition approximation," Journal of Chemical Theory and Computation 9, 20722082 (2013).
- ⁷¹F. J. Avila Ferrer, J. Cerezo, J. Soto, R. Improta, and F. Santoro, "First-principle computation of absorption and fluorescence spectra in solution accounting for vibronic structure, temperature effects and solvent inhomogeneous broadening," Computational and Theoretical Chemistry 10401041, 328337 (2014).
- ⁷²S. Hirayama and D. Phillips, "Correction for refractive index in the comparison of radiative lifetimes in vapour and solution phases," Journal of Photochemistry 12, 139–145 (1980).
- ⁷³J. R. Lakowicz, ed., *Principles of Fluorescence Spectroscopy* (Springer US, 2006).
- ⁷⁴K. A. Fletcher, S. O. Fakayode, M. Lowry, S. A. Tucker, S. L. Neal, I. W. Kimaru, M. E. McCarroll, G. Patonay, P. B. Oldham, O. Rusin, R. M. Strongin, and I. M. Warner, "Molecular fluorescence, phosphorescence, and chemiluminescence spectrometry," Analytical Chemistry 78, 4047–4068 (2006).
- ⁷⁵Y. K. Law and A. A. Hassanali, "Role of quantum vibrations on the structural, electronic, and optical properties of 9-methylguanine," The Journal of Physical Chemistry A 119, 1081610827 (2015).
- ⁷⁶S. Sappati, A. Hassanali, R. Gebauer, and P. Ghosh, "Nuclear quantum effects in a hiv/cancer inhibitor: The case of ellipticine," The Journal of Chemical Physics 145 (2016), 10.1063/1.4968046.
- ⁷⁷T. J. Zuehlsdorff, J. A. Napoli, J. M. Milanese, T. E. Markland, and C. M. Isborn, "Unraveling electronic absorption spectra using nuclear quantum effects: Photoactive yellow protein and green fluorescent protein chromophores in water," J. Chem. Phys. 149, 024107 (2018), https://doi.org/10.1063/1.5025517.
- ⁷⁸Y. Law and A. Hassanali, "The importance of nuclear quantum effects in spectral line broadening of optical spectra and electrostatic properties in aromatic chromophores," J. Chem. Phys. 148, 102331 (2018).
- ⁷⁹R. A. Marcus, "Relation between charge transfer absorption and fluorescence spectra and the inverted region," The Journal of Physical Chemistry 93, 3078–3086 (1989).
- ⁸⁰R. Zaleśny, N. A. Murugan, F. Gel'mukhanov, Z. Rinkevicius, B. Ośmiałowski, W. Bartkowiak, and H. Ågren, "Toward fully nonempirical simulations of optical band shapes of molecules in solution: A case study of heterocyclic ketoimine difluoroborates," The Journal of Physical Chemistry A 119, 5145–5152 (2014).
- ⁸¹A. Hazra, H. H. Chang, and M. Nooijen, "First principles simulation of the uv absorption spectrum of ethylene using the vertical franck-condon approach," The Journal of Chemical Physics 121, 21252136 (2004).
- ⁸²F. J. Avila Ferrer and F. Santoro, "Comparison of vertical and adiabatic harmonic approaches for the calculation of the vibrational structure of electronic spectra," Physical Chemistry Chemical Physics 14, 13549 (2012).
- ⁸³P. Macak, Y. Luo, and H. Ågren, "Simulations of vibronic profiles in two-photon absorption," Chemical Physics Letters 330, 447456 (2000).
- ⁸⁴J. Cerezo and F. Santoro, "Revisiting vertical models to simulate the line shape of electronic spectra adopting cartesian and internal coordinates," Journal of Chemical Theory and Computation 12, 49704985 (2016).
- 85 M. Biczysko, J. Bloino, F. Santoro, and V. Barone, "Time-independent approaches to simulate electronic spectra line-shapes: From small molecules to macrosystems," (2011).
- ⁸⁶F. Santoro, A. Lami, R. Improta, J. Bloino, and V. Barone, "Effective method for the computation of optical spectra of large molecules at finite temperature including the duschinsky and herzbergteller effect: The qx band of porphyrin as a case study," The Journal of Chemical Physics 128 (2008),

- 10.1063/1.2929846.
- ⁸⁷F. Santoro, C. Cappelli, and V. Barone, "Effective time-independent calculations of vibrational resonance raman spectra of isolated and solvated molecules including duschinsky and herzbergteller effects," Journal of Chemical Theory and Computation 7, 18241839 (2011).
- ⁸⁸F. J. Avila Ferrer, V. Barone, C. Cappelli, and F. Santoro, "Duschinsky, herzbergteller, and multiple electronic resonance interferential effects in resonance raman spectra and excitation profiles. the case of pyrene," Journal of Chemical Theory and Computation 9, 35973611 (2013).
- 89P. Yang, M. Pang, W. Shen, M. Li, and R. He, "Vibronic analysis of the 1lb↔s0 transitions of indole and 3-methylindole: The influence of anharmonic, duschinsky, and herzberg-teller contributions," Journal of Molecular Spectroscopy 313, 40–48 (2015).
- ⁹⁰E. R. Davidson and A. A. Jarzecki, "Zero point corrections to vertical excitation energies," Chemical Physics Letters 285, 155–159 (1998).
- ⁹¹C. Adamo and D. Jacquemin, "The calculations of excitedstate properties with time-dependent density functional theory," Chem. Soc. Rev. 42, 845856 (2013).
- ⁹²C. Fang, B. Oruganti, and B. Durbeej, "How method-dependent are calculated differences between vertical, adiabatic, and 00 excitation energies?" The Journal of Physical Chemistry A 118, 41574171 (2014).
- ⁹³X. He, V. H. Man, W. Yang, T.-S. Lee, and J. Wang, "A fast and high-quality charge model for the next generation general amber force field," The Journal of Chemical Physics 153, 114502 (2020).
- ⁹⁴C. Das, P. D. Olmsted, and M. G. Noro, "Water permeation through stratum corneum lipid bilayers from atomistic simulations," Soft Matter 5, 4549 (2009).
- ⁹⁵C. M. Isborn, A. W. Götz, M. A. Clark, R. C. Walker, and T. J. Martínez, "Electronic absorption spectra from mm and ab initio qm/mm molecular dynamics: Environmental effects on the absorption spectrum of photoactive yellow proteinn," Journal of Chemical Theory and Computation 8, 5092–5106 (2012).
- ⁹⁶L. Pejov, D. Spångberg, and K. Hermansson, "Using md snapshots in ab initio and dft calculations: Oh vibrations in the first hydration shell around li+(aq)," The Journal of Physical Chemistry A 109, 5144–5152 (2005).
- ⁹⁷G. A. Cisneros, J.-P. Piquemal, and T. A. Darden, "Quantum mechanics/molecular mechanics electrostatic embedding with continuous and discrete functions," The Journal of Physical Chemistry B 110, 13682–13684 (2006).
- ⁹⁸T. Schwabe, J. M. H. Olsen, K. Sneskov, J. Kongsted, and O. Christiansen, "Solvation effects on electronic transitions: Exploring the performance of advanced solvent potentials in polarizable embedding calculations," Journal of Chemical Theory and Computation 7, 2209–2217 (2011).
- ⁹⁹H. J. C. Berendsen, J. P. M. Postma, W. F. van Gunsteren, A. DiNola, and J. R. Haak, "Molecular dynamics with coupling to an external bath," The Journal of Chemical Physics 81, 36843690 (1984).
- ¹⁰⁰T. Yanai, D. P. Tew, and N. C. Handy, "A new hybrid exchange-correlation functional using the coulomb-attenuating method (CAM-b3lyp)," Chemical Physics Letters 393, 51–57 (2004).
- ¹⁰¹S. Hirata and M. Head-Gordon, "Time-dependent density functional theory within the tamm-dancoff approximation," Chemical Physics Letters 314, 291–299 (1999).
- 102M. E. CASIDA, "Time-dependent density functional response theory for molecules," in *Recent Advances in Density Functional Methods* (WORLD SCIENTIFIC, 1995) pp. 155–192.
- ¹⁰³S. Grimme, J. Antony, S. Ehrlich, and H. Krieg, "A consistent and accurate ab initio parametrization of density functional dispersion correction (dft-d) for the 94 elements h-pu," The Journal of Chemical Physics 132 (2010), 10.1063/1.3382344.

- ¹⁰⁴A. Chantzis, A. D. Laurent, C. Adamo, and D. Jacquemin, "Is the tamm-dancoff approximation reliable for the calculation of absorption and fluorescence band shapes?" Journal of Chemical Theory and Computation 9, 45174525 (2013).
- ¹⁰⁵A. Patra, G. B. Pipim, A. I. Krylov, and S. Mallikar-jun Sharada, "Performance of density functionals for excited-state properties of isolated chromophores and exciplexes: Emission spectra, solvatochromic shifts, and charge-transfer character," Journal of Chemical Theory and Computation 20, 25202537 (2024).
- ¹⁰⁶T. M. Henderson, A. F. Izmaylov, G. Scalmani, and G. E. Scuseria, "Can short-range hybrids describe long-range-dependent properties?" The Journal of Chemical Physics 131 (2009), 10.1063/1.3185673.
- ¹⁰⁷O. A. Vydrov and G. E. Scuseria, "Assessment of a long-range corrected hybrid functional," The Journal of Chemical Physics 125 (2006), 10.1063/1.2409292.
- ¹⁰⁸O. A. Vydrov, G. E. Scuseria, and J. P. Perdew, "Tests of functionals for systems with fractional electron number," The Journal of Chemical Physics **126** (2007), 10.1063/1.2723119.
- 109Y. Zhao and D. G. Truhlar, "The m06 suite of density functionals for main group thermochemistry, thermochemical kinetics, noncovalent interactions, excited states, and transition elements: two new functionals and systematic testing of four m06-class functionals and 12 other functionals," Theoretical Chemistry Accounts 120, 215241 (2007).
- ¹¹⁰S. Seritan, C. Bannwarth, B. S. Fales, E. G. Hohenstein, C. M. Isborn, S. I. L. Kokkila-Schumacher, X. Li, F. Liu, N. Luehr, J. W. Snyder, C. Song, A. V. Titov, I. S. Ufimtsev, L.-P. Wang, and T. J. Martínez, "Terachem: A graphical processing unit-accelerated electronic structure package for large-scale ab initio molecular dynamics," WIREs Computational Molecular Science 11 (2020), 10.1002/wcms,1494.
- ¹¹¹M. J. Frisch, G. W. Trucks, H. B. Schlegel, G. E. Scuseria, M. A. Robb, J. R. Cheeseman, G. Scalmani, V. Barone, G. A. Petersson, H. Nakatsuji, X. Li, M. Caricato, A. V. Marenich, J. Bloino, B. G. Janesko, R. Gomperts, B. Mennucci, H. P. Hratchian, J. V. Ortiz, A. F. Izmaylov, J. L. Sonnenberg, D. Williams-Young, F. Ding, F. Lipparini, F. Egidi, J. Goings, B. Peng, A. Petrone, T. Henderson, D. Ranasinghe, V. G. Zakrzewski, J. Gao, N. Rega, G. Zheng, W. Liang, M. Hada, M. Ehara, K. Toyota, R. Fukuda, J. Hasegawa, M. Ishida, T. Nakajima, Y. Honda, O. Kitao, H. Nakai, T. Vreven, K. Throssell, J. A. Montgomery, Jr., J. E. Peralta, F. Ogliaro, M. J. Bearpark, J. J. Heyd, E. N. Brothers, K. N. Kudin, V. N. Staroverov, T. A. Keith, R. Kobayashi, J. Normand, K. Raghavachari, A. P. Rendell, J. C. Burant, S. S. Iyengar, J. Tomasi, M. Cossi, J. M. Millam, M. Klene, C. Adamo, R. Cammi, J. W. Ochterski, R. L. Martin, K. Morokuma, O. Farkas, J. B. Foresman, and D. J. Fox, "Gaussian~16 Revision C.01," (2016), gaussian Inc. Wallingford CT.
- ¹¹²E. Cancès, B. Mennucci, and J. Tomasi, "A new integral equation formalism for the polarizable continuum model: Theoretical background and applications to isotropic and anisotropic dielectrics," The Journal of Chemical Physics 107, 30323041 (1997).
- ¹¹³B. Mennucci, E. Cancès, and J. Tomasi, "Evaluation of solvent effects in isotropic and anisotropic dielectrics and in ionic solutions with a unified integral equation method: Theoretical bases, computational implementation, and numerical applications," The Journal of Physical Chemistry B 101, 1050610517 (1997).
- ¹¹⁴E. Cancès and B. Mennucci, Journal of Mathematical Chemistry 23, 309326 (1998).
- ¹¹⁵G. Scalmani and M. J. Frisch, "Continuous surface charge polarizable continuum models of solvation. i. general formalism," The Journal of Chemical Physics 132 (2010), 10.1063/1.3359469.
- ¹¹⁶B. Mennucci, "Polarizable continuum model," WIREs Computational Molecular Science 2, 386404 (2012).

- ¹¹⁷S. Uchiyama, K. Kimura, C. Gota, K. Okabe, K. Kawamoto, N. Inada, T. Yoshihara, and S. Tobita, "Environmentsensitive fluorophores with benzothiadiazole and benzoselenadiazole structures as candidate components of a fluorescent polymeric thermometer," Chemistry - A European Journal 18, 9552–9563 (2012).
- ¹¹⁸K. Imai, S. Uzu, and T. Toyo'oka, "Fluorogenic reagents having benzofuran structure in liquid chromatography," Journal of Pharmaceutical and Biomedical Analysis 7, 1395–1403 (1989).
- ¹¹⁹J. Rumin, H. Bonnefond, B. Saint-Jean, C. Rouxel, A. Sciandra, O. Bernard, J.-P. Cadoret, and G. Bougaran, "The use of fluorescent nile red and BODIPY for lipid measurement in microalgae," Biotechnology for Biofuels 8 (2015), 10.1186/s13068-015-0220-4.
- ¹²⁰G. S. Alemán-Nava, S. P. Cuellar-Bermudez, M. Cuaresma, R. Bosma, K. Muylaert, B. E. Ritmann, and R. Parra, "How to use nile red, a selective fluorescent stain for microalgal neutral lipids," Journal of Microbiological Methods 128, 74–79 (2016).
- ¹²¹C. G. Knight, "Stereospecific synthesis of l-2-amino-3-(7-methoxy-4-coumaryl)propionic acid, an alternative to tryptophan in quenched fluorescent substrates for peptidases," Letters in Peptide Science 5, 1–4 (1998).
- ¹²²L. E. Yandek, A. Pokorny, A. Florén, K. Knoelke, Ülo Langel, and P. F. Almeida, "Mechanism of the cell-penetrating peptide transportan 10 permeation of lipid bilayers," Biophysical Journal 92, 2434–2444 (2007).
- ¹²³I. Tosi, M. Segado Centellas, E. Campioli, A. Iagatti, A. Lapini, C. Sissa, L. Baldini, C. Cappelli, M. Di Donato, F. Sansone, F. Santoro, and F. Terenziani, "Excitation dynamics in heterobichromophoric calixarene systems," ChemPhysChem 17, 1686–1706 (2016).
- ¹²⁴J. M. Dixon, M. Taniguchi, and J. S. Lindsey, "PhotochemCAD 2. a refined program with accompanying spectral database for photochemical calculations," Photochemistry and Photobiology (2004), 10.1562/2004-11-06-tsn-361.
- ¹²⁵R. Farinotti, P. Siard, J. Bourson, S. Kirkiacharian, B. Valeur, and G. Mahuzier, "4-bromomethyl-6, 7-dimethoxycoumarin as a fluorescent label for carboxylic acids in chromatographic detection," Journal of Chromatography A 269, 8190 (1983).
- ¹²⁶T. R. Nelson, A. J. White, J. A. Bjorgaard, A. E. Sifain, Y. Zhang, B. Nebgen, S. Fernandez-Alberti, D. Mozyrsky, A. E. Roitberg, and S. Tretiak, "Non-adiabatic excited-state molecular dynamics: Theory and applications for modeling photophysics in extended molecular materials," Chemical Reviews 120, 22152287 (2020).
- ¹²⁷A. J. Dunnett, D. Gowland, C. M. Isborn, A. W. Chin, and T. J. Zuehlsdorff, "Influence of non-adiabatic effects on linear absorption spectra in the condensed phase: Methylene blue," The Journal of Chemical Physics 155, 144112 (2021), https://pubs.aip.org/aip/jcp/article-pdf/doi/10.1063/5.0062950/13306941/144112_l_online.pdf.
- ¹²⁸S. Mazères, V. Schram, J. Tocanne, and A. Lopez, "7-nitrobenz-2-oxa-1, 3-diazole-4-yl-labeled phospholipids in lipid membranes: differences in fluorescence behavior," Biophysical Journal 71, 327–335 (1996).
- ¹²⁹H. A. L. Filipe, M. J. Moreno, and L. M. S. Loura, "Interaction of 7-nitrobenz-2-oxa-1,3-diazol-4-yl-labeled fatty amines with 1-palmitoyl, 2-oleoyl-sn-glycero-3-phosphocholine bilayers: A molecular dynamics study," The Journal of Physical Chemistry B 115, 10109-10119 (2011).
- ¹³⁰J. R. Robalo, J. P. P. Ramalho, and L. M. S. Loura, "NBD-labeled cholesterol analogues in phospholipid bilayers: Insights from molecular dynamics," The Journal of Physical Chemistry B 117, 13731–13742 (2013).
- ¹³¹S. E. Pidgeon, J. M. Fura, W. Leon, M. Birabaharan, D. Vezenov, and M. M. Pires, "Metabolic profiling of bacteria by unnatural c-terminated d-amino acids," Angewandte Chemie International Edition 54, 6158–6162 (2015).
- ¹³²C. Jiang, H. Huang, X. Kang, L. Yang, Z. Xi, H. Sun, M. D. Pluth, and L. Yi, "NBD-based synthetic probes for sensing

- small molecules and proteins: design, sensing mechanisms and biological applications," Chemical Society Reviews **50**, 7436–7495 (2021).
- ¹³³S. Uchiyama, T. Santa, T. Fukushima, H. Homma, and K. Imai, "Effects of the substituent groups at the 4- and 7-positions on the fluorescence characteristics of benzofurazan compounds," Journal of the Chemical Society, Perkin Transactions 2, 2165– 2174 (1998).
- ¹³⁴S. Fery-Forgues, J.-P. Fayet, and A. Lopez, "Drastic changes in the fluorescence properties of NBD probes with the polarity of the medium: involvement of a TICT state?" Journal of Photochemistry and Photobiology A: Chemistry 70, 229–243 (1993).
- ¹³⁵Y. Lee, I. Yang, J. E. Lee, S. Hwang, J. W. Lee, S.-S. Um, T. L. Nguyen, P. J. Yoo, H. Y. Woo, J. Park, and S. K. Kim, "Enhanced photocurrent generation by förster resonance energy transfer between phospholipid-assembled conjugated oligoelectrolytes and nile red," The Journal of Physical Chemistry C 117, 3298–3307 (2013).
- ¹³⁶D. Basting, D. Ouw, and F. Schäfer, "The phenoxazones: A new class of laser dyes," Optics Communications 18, 260–262 (1976).
- ¹³⁷R. Plenderleith, T. Swift, and S. Rimmer, "Highly-branched poly(n-isopropyl acrylamide)s with core–shell morphology below the lower critical solution temperature," RSC Adv. 4, 50932–50937 (2014).
- ¹³⁸M. M. Davis and H. B. Helzer, "Titrimetric and equilibrium studies using indicators related to nile blue a." Analytical Chemistry 38, 451–461 (1966).
- ¹³⁹L. O. Kostjukova, S. V. Leontieva, and V. V. Kostjukov, "The vibronic absorption spectrum and electronic states of nile red in aqueous solution," ChemistrySelect 6, 12971304 (2021).
- ¹⁴⁰B. Boldrini, E. Cavalli, A. Painelli, and F. Terenziani, "Polar dyes in solution: A joint experimental and theoretical study of absorption and emission band shapes," The Journal of Physical

- Chemistry A 106, 62866294 (2002).
- ¹⁴¹A. Ciencialová, L. Žáková, J. Jiráček, J. Barthová, and T. Barth, "Preparation and characterization of two LysB29 specifically labelled fluorescent derivatives of human insulin," Journal of Peptide Science 10, 470–478 (2004).
- ¹⁴²F. No, S. Olsson, J. Khler, and H. Wu, "Boltzmann generators: Sampling equilibrium states of many-body systems with deep learning," Science 365 (2019), 10.1126/science.aaw1147.
- ¹⁴³V. L. Deringer, M. A. Caro, and G. Csnyi, "Machine learning interatomic potentials as emerging tools for materials science," Advanced Materials 31 (2019), 10.1002/adma.201902765.
- ¹⁴⁴S. Doerr, M. Majewski, A. Prez, A. Krmer, C. Clementi, F. Noe, T. Giorgino, and G. De Fabritiis, "Torchmd: A deep learning framework for molecular simulations," Journal of Chemical Theory and Computation 17, 23552363 (2021).
- ¹⁴⁵R. Galvelis, A. Varela-Rial, S. Doerr, R. Fino, P. Eastman, T. E. Markland, J. D. Chodera, and G. De Fabritiis, "Nnp/mm: Accelerating molecular dynamics simulations with machine learning potentials and molecular mechanics," Journal of Chemical Information and Modeling 63, 57015708 (2023).
- ¹⁴⁶V. Barone, M. Fus, R. Aguado, S. Potenti, I. Len, E. R. Alonso, S. Mata, F. Lazzari, G. Mancini, L. Spada, A. Gualandi, P. G. Cozzi, C. Puzzarini, and J. L. Alonso, "Bringing machinelearning enhanced quantum chemistry and microwave spectroscopy to conformational landscape exploration: the paradigmatic case of 4fluorothreonine," Chemistry A European Journal 29 (2023), 10.1002/chem.202203990.
- ¹⁴⁷V. Barone, M. Fus, F. Lazzari, and G. Mancini, "Benchmark structures and conformational landscapes of amino acids in the gas phase: A joint venture of machine learning, quantum chemistry, and rotational spectroscopy," Journal of Chemical Theory and Computation 19, 12431260 (2023).